1 Sources and characteristics of size-resolved particulate organic acids and methanesulfonate in a
2 coastal megacity: Manila, Philippines

3 Connor Stahl[1], Melliza Templonuevo Cruz[2,3], Paola Angela Bañaga[2,4], Grace Betito[2,4], Rachel A.
4 Braun[1], Mojtaba Azadi Aghdam[1], Maria Obiminda Cambaliza[2,4], Genevieve Rose Lorenzo[2,5],
5 Alexander B. MacDonald[1], Miguel Ricardo A. Hilario[2], Preciosa Corazon Pabroa[6], John Robin
6 Yee[6], James Bernard Simpas[2,4], Armin Sorooshian[1,5]

7 [1]Department of Chemical and Environmental Engineering, University of Arizona, Tucson,
8 Arizona, 85721, USA
9 [2]Manila Observatory, Quezon City, 1108, Philippines
10 [3]Institute of Environmental Science and Meteorology, University of the Philippines, Diliman,
11 Quezon City, 1101, Philippines
12 [4]Department of Physics, School of Science and Engineering, Ateneo de Manila University,
13 Quezon City, 1108, Philippines
14 [5]Department of Hydrology and Atmospheric Sciences, University of Arizona, Tucson, Arizona,
15 85721, USA
16 [6] Philippine Nuclear Research Institute - Department of Science and Technology,
17 Commonwealth Avenue, Diliman, Quezon City, 1101, Philippines

18 *Correspondence to: armin@email.arizona.edu*

19   **Abstract**

20   A 16-month (July 2018 – October 2019) dataset of size-resolved aerosol composition is used to
21   examine the sources and characteristics of five organic acids (oxalate, succinate, adipate,
22   maleate, phthalate) and methanesulfonate (MSA) in Metro Manila, Philippines. As one of the
23   most polluted megacities globally, Metro Manila offers a view of how diverse sources and
24   meteorology impact the relative amounts and size distributions of these species. A total of 66
25   sample sets were collected with a Micro-Orifice Uniform Deposit Impactor (MOUDI), of which
26   54 sets were analyzed for composition. Organic acids and MSA surprisingly were less abundant
27   than in other global regions that are also densely populated. The combined species accounted for
28   an average of 0.80 ± 0.66 % of total gravimetric mass between 0.056 and 18 μm, leaving still
29   33.74 % of mass unaccounted for after considering black carbon and water-soluble ions and
30   elements. The unresolved mass is suggested to consist of non-water-soluble metals as well as
31   both water-soluble and non-water-soluble organics. Oxalate was approximately an order of
32   magnitude more abundant than the other five species (149 ± 94 ng m^{-3} versus others being < 10
33   ng m^{-3}) across the 0.056 – 18 μm size range. Both positive matrix factorization (PMF) and
34   correlation analysis is conducted with tracer species to investigate the possible sources for
35   organic acids and MSA. Enhanced biomass burning influence in the 2018 southwest monsoon
36   resulted in especially high levels of submicrometer succinate, MSA, oxalate, and phthalate.
37   Peculiarly, MSA had negligible contributions from marine sources but instead was linked to
38   biomass burning and combustion. Enhanced precipitation during the two monsoon seasons (8
39   June – 4 October 2018 and 14 June – 7 October 2019) coincided with stronger influence from
40   local emissions rather than long-range transport, leading to notable concentration enhancements
41   in both the sub- and supermicrometer ranges for some species (e.g., maleate and phthalate).
42   While secondary formation via gas-to-particle conversion is consistent with submicrometer
43   peaks for the organic acids and MSA, several species (i.e., phthalate, adipate, succinate, oxalate)
44   exhibited a prominent peak in the coarse mode, largely owing to their association with crustal
45   emissions (i.e., more alkaline aerosol type) rather than sea salt. Oxalate's strong association with
46   sulfate in the submicrometer mode supports an aqueous-phase formation pathway for the study
47   region. However, high concentrations during periods of low rain and high solar radiation
48   suggests photo-oxidation is an important formation pathway.

1. Introduction

Organic acids are ubiquitous components of ambient particulate matter and can contribute appreciably to total mass concentrations in diverse regions ranging from the Arctic to deserts (e.g., Barbaro et al., 2017; Gao et al., 2003; Kawamura et al., 2005). Furthermore, another class of species contributing to ambient aerosol mass is organosulfur compounds, with methanesulfonate (MSA) being an example species (Bardouki et al., 2003b; Ding et al., 2017; Falkovich et al., 2005; Kerminen et al., 1999; Maudlin et al., 2015; Ziemba et al., 2011). The spatiotemporal and size-resolved mass concentration profiles of organic and sulfonic acids are difficult to characterize and can significantly vary depending on the time of day, season, region, and meteorological profile (Adam et al., 2020; Bagtasa et al., 2019; Kobayashi et al., 2004; Maudlin et al., 2015; Mochida et al., 2003; Reid et al., 2013). It is necessary to quantify their relative abundances, and to understand factors affecting their production and eventual removal to be able to quantify their influence on aerosol hygroscopic and optical properties (Beaver et al., 2008; Cai et al., 2017; Freedman et al., 2009; Marsh et al., 2017; Marsh et al., 2019; Myhre and Nielsen, 2004; Peng et al., 2016; Xue et al., 2009). Low molecular weight organic acids are water-soluble and can range widely in hygroscopicity when in their pure salt form depending on factors such as carbon number (Prenni et al., 2001; Saxena and Hildemann, 1996; Sorooshian et al., 2008) and interactions with other components in multi-component aerosol particles (Drozd et al., 2014).

Organic acids are generally believed to effectively scatter light and have a cooling effect on climate (McGinty et al., 2009; Myhre and Nielsen, 2004), although their overall impact on properties such as refractive index in multicomponent aerosols is poorly characterized. Refractive indices for species investigated in this work range widely from 1.43 (MSA) to 1.62 (phthalic acid). MSA is assumed to be purely scattering similar to sulfate (Hodshire et al., 2019) and to have hygroscopic properties close to those of ammonium sulfate (Asmi et al., 2010; Fossum et al., 2018). However, its hygroscopic and optical behavior is not fully understood, and is still an active area of research (Liu et al., 2011; Peng and Chan, 2001; Tang et al., 2019; Tang et al., 2015; Zeng et al., 2014).

Decades of research into atmospheric organic acids and MSA have yielded rich insights into their sources, production mechanisms, and fate in the atmosphere (Baboukas et al., 2000; Bardouki et al., 2003a; Gondwe et al., 2004; Kawamura and Bikkina, 2016; Limbeck et al., 2001; Norton et al., 1983; Ovadnevaite et al., 2014; Sorooshian et al., 2009; van Pinxteren et al., 2015). MSA is produced predominantly from the oxidation of dimethylsulfide (DMS) emitted from oceans (Bates et al., 2004; Davis et al., 1998; Kerminen et al., 2017), but it also can be linked to biomass burning, urban, and agricultural emissions (Sorooshian et al., 2015). Sources of organic acids include primary emissions from biomass burning, biogenic activity, and the combustion of fossil fuels (Kawamura and Kaplan, 1987) and secondary formation via gas-to-particle conversion processes stemming from both biogenic (Carlton et al., 2006) and anthropogenic emissions (Sorooshian et al., 2007b). Secondary processing can include both aqueous phase chemistry in clouds (Blando and Turpin, 2000; Ervens, 2018; Ervens et al., 2014; Hoffmann et al., 2019; Rose et al., 2018; Sareen et al., 2016; Warneck, 2005) and photo-

90   oxidation of volatile organic compounds (VOCs) in cloud-free air (Andreae and Crutzen, 1997;
91   Gelencsér and Varga, 2005). These various sources and production pathways result in mono- and
92   dicarboxylic acids being prevalent across a range of aerosol sizes (Bardouki et al., 2003b;
93   Kavouras and Stephanou, 2002; Neusüss et al., 2000; Yao et al., 2002). Little is reported in terms
94   of the size-resolved nature of organic acids and MSA over long periods (> 6 months) of time
95   with high sampling frequency (weekly or better). Although insights have already been gathered
96   from size-resolved measurement studies (Table S1), most measurement reports are based on bulk
97   mass concentration measurements (Chebbi and Carlier, 1996; Kawamura and Bikkina, 2016).
98   Studying the seasonal variations of size-resolved organic acid and MSA aerosols could prove
99   vital in improved understanding of their formation and removal mechanisms, and associated
100 sensitivity to seasonally dependent sources and meteorological factors.

101 The Philippines is an important region to study aerosols due to the wide range in both
102 meteorological conditions and diverse local and regional emissions sources (Alas et al., 2018;
103 Bagtasa and Yuan, 2020; Braun et al., 2020; Hilario et al., 2020a; Kecorius et al., 2017). In
104 addition to aerosol sources from nearby regions (Hilario et al., 2020b), the Philippines also has a
105 significant source of local pollution largely consisting of vehicular emissions due to high
106 population density (Madueño et al., 2019), the use of outdated vehicles (Biona et al., 2017), ship
107 exhaust from high density shipping lanes (Streets et al., 1997; Streets et al., 2000), and more
108 lenient air regulations leading to significant air pollution due to rapid growth and urbanization
109 (Alas et al., 2018; Kecorius et al., 2017). This leads to Metro Manila containing some of the
110 highest black carbon (BC) concentrations in Southeast Asia, and quite possibly the world (Alas
111 et al., 2018; Hopke et al., 2011; Kecorius et al., 2017; Kim Oanh et al., 2006). Past aerosol
112 characterization work for that region has focused mainly on gravimetric analysis for total bulk
113 mass (e.g., $PM_{2.5}$, PM_{10}) (Bagtasa et al., 2018; Bagtasa et al., 2019; Cohen et al., 2009; Kim
114 Oanh et al., 2006), water-soluble inorganic and organic ion speciation (AzadiAghdam et al.,
115 2019; Braun et al., 2020; Cruz et al., 2019; Kim Oanh et al., 2006; Simpas et al., 2014; Stahl et
116 al., 2020a), and BC analysis (Alas et al., 2018; Bautista et al., 2014; Kecorius et al., 2017;
117 Takahashi et al., 2014). In an analysis of two size-resolved aerosol sets in Manila, a significant
118 portion of the total mass unaccounted for by the water-soluble inorganic, water-soluble organic,
119 and BC components was attributed to (but not limited to) organics and non-water soluble metals
120 (Cruz et al., 2019). However, a concentrated effort to characterize the contributions of the water-
121 soluble organic acids to the total aerosol mass in Manila over the course of a full year has not
122 been undertaken.

123 The aim of this study is to use a 16 month-long dataset of size-resolved composition in Quezon
124 City in Metro Manila to address the following questions: (i) how much do organic acids and
125 MSA contribute to the region's aerosol mass concentrations?; (ii) what are the seasonal
126 differences in the mass size distribution profile of organic acids and MSA, and what drives the
127 changes?; and (iii) what are the sources and predominant formation mechanisms of these species
128 in the sub- and super-micrometer diameter ranges? The results of this study are put in broad
129 context by comparing findings to those in other regions.

130

2. Methods

2.1 Study site description

Metro Manila is comprised of 16 cities and a municipality totaling to a population of about 12.9 million people and a collective population density of 20,800 km^{-2} (Alas et al., 2018; PSA, 2016). Quezon City is the most populated city in Metro Manila containing 2.94 million people with a population density of 18,000 km^{-2} (PSA, 2016), which is amidst the highest in the world. Because of these reasons, Metro Manila is a fitting location for examining locally produced anthropogenic aerosols superimposed on a variety of other marine and continentally influenced air masses transported from upwind regions (Kim Oanh et al., 2006).

Measurements were conducted over a 16-month period between July 2018 and October 2019 at Manila Observatory (MO; 14.64° N, 121.08° E) on the third floor (~85 m a.s.l.) of an office building, which is on the Ateneo de Manila University campus in Quezon City, Philippines (Fig. 1). Sampling was conducted approximately 100 m away from the nearest road on campus and therefore campus emissions do not impact sampling to a large degree, qualifying the monitoring site as an urban mixed background site (Hilario et al., 2020a) capturing local, regional, and long-range transported emissions. The following four seasons were the focus of the sampling period: the 2018 southwest monsoon (SWM18, 8 June – 4 October 2018) (PAGASA, 2018b, a), a transitional period (Transitional, 5 – 25 October 2018), the northeast monsoon (NEM, 26 October 2018 – 13 June 2019) (PAGASA, 2018c), and the 2019 southwest monsoon (SWM19, 14 June – 7 October 2019) (PAGASA, 2019a, b). These seasons have also been defined in other works (i.e., Akasaka et al., 2007; Cruz et al., 2013; Matsumoto et al., 2020) and can predominately be separated into two general seasons, wet (SWM) and dry (NEM). Generally, there is a second transitional period in May that transitions between the NEM and SWM (Bagtasa and Yuan, 2020), however, recent studies suggest that the transition is abrupt (Matsumoto et al., 2020). Consequently, the second transitional period was combined with the NEM season.

2.2 Instrument description

Ambient aerosol was collected with a Micro-Orifice Uniform Deposit Impactor II (MOUDI II 120R, MSP Corporation, Marple et al. (2014)) using Teflon substrates (PTFE membrane, 2 μm pores, 46.2 mm diameter, Whatman). The MOUDI-II is a 10-stage impactor with aerodynamic cutpoint diameters (D_p) of 10, 5.6, 3.2, 1.8, 1.0, 0.56, 0.32, 0.18, 0.10, and 0.056 μm with a nominal flow rate of ~30 L min^{-1}. A total of 66 MOUDI sets were collected on a weekly basis usually over a 48-hour period; however, only 54 sets where analyzed for ions and 47 of those sets were also analyzed for elements. A 48-hour period was chosen because it offered an optimal compromise between gathering samples with fine temporal resolution and samples with a sufficiently large chemical signal to exceed analytical limits of detection. Details of the sample sets are shown in Table S2 can be found in more detail in Stahl et al. (2020a), but a brief summary of the storage and extraction methods will be described here. Substrates were stored in a freezer at -20 °C after samples were collected from the MOUDI until extractions could be carried out, which on average was approximately 2 weeks. The stored substrates were then

171   extracted by sonication in Milli-Q water (18.2 MΩ-cm) for 30 minutes. After sonication,
172   solutions were immediately analyzed to prevent degradation while the remaining extracts were
173   stored in a refrigerator for additional analyses. There have been studies that discuss the effects of
174   sonication oxidation degrading organic species (i.e., Miljevic et al., 2014). It was determined
175   through experimental tests that no significant degradation occurred during the sonication process
176   for the species being analyzed in this study.

177   Water-soluble organic acids, MSA, and inorganic ions were speciated and quantified using ion
178   chromatography (IC; Thermo Scientific Dionex ICS-2100 system) with a flowrate of 0.4 mL
179   min^{-1}. The anionic species of relevance to this study were MSA, chloride (Cl^-), nitrate (NO_3^-),
180   sulfate (SO_4^{2-}), adipate, succinate, maleate, oxalate, and phthalate. These anions were resolved
181   using potassium hydroxide (KOH) eluent, an AS11-HC 250 mm column, and an AERS 500e
182   suppressor. The cationic species of relevance to this study was sodium (Na^+), which was detected
183   using methanesulfonic acid eluent, a CS12A 250 mm column, and a CERS 500e suppressor. The
184   IC instrument methods for anion and cation analysis can be found in Stahl et al. (2020a). Water-
185   soluble elements were measured using a triple quadrupole inductively coupled plasma mass
186   spectrometry (ICP-QQQ; Agilent 8800 Series). The quantified elements of relevance to this
187   study include Al, As, Cd, K, Ni, Pb, Rb, Ti, and V. Limits of detection (LOD) and recoveries
188   were calculated for all ionic and elemental species and provided in Table S3. Aside from the
189   species that are the focus of this study (organic acids and MSA), the other elements and ions
190   were included as they are useful tracers for different aerosol sources to aid in source
191   apportionment. Although pyruvate was speciated with IC, it is not considered with the other
192   organic acids because it was below the LOD for 48 of the 54 sets. It should also be noted that
193   only a subset of species used for analyses were listed here. The full suite of species can be seen
194   in Stahl et al. (2020a).

195   Eleven of the 66 MOUDI sets included simultaneously operated MOUDIs next to each other to
196   complement the chemical speciation analysis with gravimetric analysis. A Sartorius ME5-F
197   microbalance (sensitivity of ± 1 μg) was used in an air-buffered room with controlled
198   temperature (20 – 23 °C) and relative humidity (RH: 30 – 40 %). Each substrate was passed near
199   an antistatic tip for approximately 30 seconds to minimize bias due to electrostatic charge.
200   Multiple weight measurements were conducted before and after sampling, with the difference
201   between weighings being less than 10 μg for each condition, respectively. The difference
202   between substrate weights before and after sampling was equated to total gravimetric mass.

203   Black carbon was measured using a Multi-wavelength Absorption Black Carbon Instrument
204   (MABI; Australian Nuclear Science and Technology Organisation). The MABI optically
205   quantifies black carbon concentrations by detecting the absorption at seven wavelengths (405,
206   465, 525, 639, 870, 940, and 1050 nm); however, the wavelength at 870 nm is used here as black
207   carbon is the primary absorber at that wavelength (Cruz et al., 2019; Ramachandran and Rajesh,
208   2007; Ran et al., 2016).

209   Meteorological parameters were measured at MO during the study period using a Davis Vantage
210   Pro2[TM] Plus automatic weather station, which was located on the roof. Measured parameters of
211   relevance included temperature, accumulated rain, RH, and solar radiation. Data were collected

212   in five-minute increments and were cleaned based on the method of Bañares et al. (2018) to
213   verify values were in acceptable ranges. The meteorological parameters, except for rain, were
214   averaged over each sampling period while rain was summed over time to obtain the accumulated
215   precipitation for a sampling period. There were two periods where the automatic weather station
216   located at MO had missing values, 6 November – 27 November 2018 and 7 August – 3
217   September 2019. In these cases, missing values were substituted with values from a secondary
218   automatic weather station located approximately 2 km away (14.63° N, 121.06° E), and if
219   missing data still persisted, a tertiary station located 5 km away (14.67° N, 121.11° E) was used.
220   Identical data cleaning procedures were implemented for the secondary and tertiary sites.

221

222   2.3 Concentration weighted trajectories (CWT)

223   A CWT analysis was conducted to identify sources of detected species. The method assigns a
224   weighted concentration to a grid that is calculated by finding the mean of sample concentrations
225   that have trajectories crossing a particular cell in the grid (e.g., Dimitriou, 2015; Dimitriou et al.,
226   2015; Hilario et al., 2020a; Hsu et al., 2003). The software TrajStat (Wang et al., 2009)
227   determines CWT profiles by using back-trajectories from the NOAA Hybrid Single-Particle
228   Lagrangian Integrated Trajectory (HYSPLIT) model (Rolph et al., 2017; Stein et al., 2015).
229   Three-day back-trajectories were obtained with an ending altitude of 500 m above ground level
230   using the Global Data Assimilation System (GDAS) and the "Model vertical velocity" method.
231   The choice of 500 m is based on representativeness of the mixed layer and having been widely
232   used in other studies (e.g., Crosbie et al., 2014; Mora et al., 2017; Sorooshian et al., 2011).
233   Trajectories were obtained every 6 hours after MOUDI sampling began for each sample set,
234   yielding approximately nine trajectories per set. A grid domain of 95° to 150° E longitude and -
235   5° to 45° N latitude was used with a grid cell resolution of 0.5° × 0.5°. The analysis was
236   performed for each measured organic acid and MSA for the full diameter range of MOUDI sets
237   (0.056 – 18 μm). A weighting function was applied to the CWT plots to minimize uncertainty.

238

239   2.4 Positive matrix factorization (PMF)

240   PMF analysis was applied to identify sources and their relative importance for the mass
241   concentration budgets of the species discussed in this work (Paatero and Tapper, 1994). Model
242   simulations were conducted based on MOUDI data for the diameter range of 0.056 – 18 μm.
243   Nineteen species (Al, Ti, K, Rb, V, Ni, As, Cd, Pb, Na^+, Cl^-, NO_3^-, SO_4^{2-}, MSA, adipate,
244   succinate, maleate, oxalate, and phthalate) were included in the analysis and categorized as
245   "strong". Each individual stage of MOUDI sets was considered an independent variable for the
246   analysis. Missing values or values below detection limit were replaced with zeros with the
247   exception of sets where ICP-QQQ analysis was not performed (57, 59, 60, 61, 62, 64, 65). Those
248   missing values were replaced with the geometric mean for each respective stage. The uncertainty
249   for each stage and species was calculated as follows:

250   $Uncertainty = 0.05 * [x] + LOD$ (Eq. 1)

251 where [x] is the concentration of the species (Reff et al., 2007). No additional uncertainty was
252 added to account for any unconsidered errors for all species. The uncertainty of the model output
253 was evaluated using displacement (DISP), bootstrapping (BS), and bootstrapping with
254 displacement (BS-DISP). For BS, 100 resamples were used and a value of 0.6 was used as a
255 threshold for the correlation coefficient (r) to pass as successful mapping for each simulation.

256 To qualify as a valid result, reported PMF results had to meet the following criteria: (i) factors
257 mapped with BS runs, (ii) no factor swaps in DISP, (iii) dQ values being close or equal to 0%,
258 and (iv) no factor swaps in BS-DISP where Al, Ti, K, Rb, V, Ni, As, Cd, Pb, Na^+, Cl^-, NO_3^-, and
259 SO_4^{2-} were displaced. PMF diagnostics can be seen in Table S4 based on the method of Brown et
260 al. (2015).

261

262 **3. Background on Measured Acids**

263 A brief overview of the species being examined is first provided before reviewing concentration
264 statistics. MSA is an oxidation product of dimethylsulfide (DMS) emitted primarily from the
265 ocean (Berresheim, 1987; Saltzman et al., 1983), but it can also be formed from dimethyl
266 sulphoxide (DMSO) emitted from anthropogenic sources such as industrial waste (Yuan et al.,
267 2004). Gaseous MSA can become associated with particulate matter via new particle formation
268 (Dawson et al., 2012), and through heterogeneous reactions or condensation onto existing
269 particles (De Bruyn et al., 1994; Hanson, 2005).

270 Of the three saturated dicarboxylic acids, succinate (C_4) and adipate (C_6) are larger chain
271 dicarboxylic acids linked to ozonolysis of cyclic alkenes, which is common in areas with
272 extensive vehicular emissions (Grosjean et al., 1978; Hatakeyama et al., 1987). They can also be
273 emitted via processes such as meat cooking (Rogge et al., 1993) and biomass burning
274 (Kawamura et al., 2013; Pereira et al., 1982) and can be secondarily formed by the photo-
275 oxidation of higher chain organic acids, such as azelaic acid (Bikkina et al., 2014; Ervens et al.,
276 2004). Oxalate (C_2) is the smallest of those three acids and is usually the most abundant on a
277 mass basis of all dicarboxylic acids in tropospheric aerosols as it represents an end-product in the
278 oxidation of both larger-chain carboxylic acids and also glyoxylic acid (Ervens et al., 2004). It
279 can be emitted via direct emissions such as from biomass burning (Graham et al., 2002;
280 Narukawa et al., 1999; Xu et al., 2020), combustion exhaust (Kawamura and Kaplan, 1987;
281 Kawamura and Yasui, 2005; Wang et al., 2010), and from various biogenic sources (Kawamura
282 and Kaplan, 1987).

283 Maleate (C_4) is an unsaturated dicarboxylic acid originating from combustion engines, including
284 via direct emissions (Kawamura and Kaplan, 1987) and secondarily produced from the photo-
285 oxidation of benzene (Rogge et al., 1993). Lastly, phthalate (C_8) represents an aromatic
286 dicarboxylic acid associated with incomplete combustion of vehicular emissions (Kawamura and
287 Kaplan, 1987) and oxidation of naphthalene or other polycyclic aromatic hydrocarbons (Fine et
288 al., 2004; Kawamura and Ikushima, 2002; Kawamura and Yasui, 2005). However, it has also
289 been linked to biomass burning (Kumar et al., 2015) and burning of plastic material such as
290 polyvinyl chloride (PVC) products, garbage, and plastic bags (Agarwal et al., 2020; Claeys et al.,

291 2012; Fu et al., 2012; Li et al., 2019; Nguyen et al., 2016; Simoneit et al., 2005). Secondary
292 formation via aqueous-phase chemistry has been documented for these organic acids (Kunwar et
293 al., 2019; Sorooshian et al., 2007a; Sorooshian et al., 2010; Sorooshian et al., 2006; Wonaschuetz
294 et al., 2012) and MSA (Hoffmann et al., 2016).

295

296 **4. Results**

297 4.1 Meteorology and Transport Patterns

298 Meteorological data are summarized based on average values temporally coincident with each
299 MOUDI sample set period for each of the seasons. The exception to this was the accumulated
300 rainfall, which was summed for the MOUDI set duration. Temperatures were stable during the
301 different seasons: 28.0 ± 1.04 °C (SWM18), 28.9 ± 0.8 °C (Transitional), 28.3 ± 1.9 °C (NEM),
302 and 28.4 ± 1.5 °C (SWM19). Solar radiation was the highest during the Transitional ($279.61 \pm$
303 19.68 W m^{-2}) and NEM (304.01 ± 67.54 W m^{-2}) seasons, and lowest during the SWM18 (225.32
304 ± 56.26 W m^{-2}) and SWM19 (256.05 ± 86.88 W m^{-2}) seasons owing largely to more cloud cover.
305 Accumulated rain was highest for both SWM seasons (SWM18: 29.78 ± 27.28 mm; SWM19:
306 16.66 ± 23.98 mm) and much lower during the Transitional (1.00 ± 1.11 mm) and NEM ($2.20 \pm$
307 6.70 mm) seasons. Relative humidity was relatively consistent across seasons: SWM18 ($69.6 \pm$
308 5.0 %), Transitional (69.2 ± 2.2 %), NEM season (62.4 ± 8.0 %), SWM19 (72.6 ± 11.7 %).
309 Finally, Fig. 1 summarizes predominant wind patterns for each season based on HYSPLIT back-
310 trajectories collected every 6 hours during sampling periods. The SWM18 and SWM19 seasons
311 were characterized by predominantly southwesterly winds, while the NEM and Transitional
312 seasons experienced mostly northeasterly winds. In conclusion, there was much higher potential
313 for wet scavenging during the SWM seasons, with the potential for more photochemical
314 reactivity in the NEM and Transitional seasons owing to enhanced incident solar radiation. As
315 humidity was generally enhanced year-round, there was the likelihood of aqueous-phase
316 processing to occur in all seasons. The combination of sustained RH, low boundary layer height,
317 and high surface-level particle concentrations have been suggested to counteract the effects of
318 wet deposition on total particle concentration in Metro Manila (Hilario et al., 2020a).

319

320 4.2 Bulk aerosol measurements

321 The range, mean, and standard deviation of concentrations integrated across the MOUDI
322 diameter range ($0.056 - 18$ μm) are shown in Table 1 for each organic acid and MSA for all
323 seasons. In order of decreasing concentration, the following was the order of abundance based on
324 the cumulative dataset: oxalate (149 ± 94 ng m^{-3}) > succinate (10 ± 22 ng m^{-3}) > maleate ($10 \pm$
325 20 ng m^{-3}) > phthalate (9 ± 14 ng m^{-3}) > adipate (7.6 ± 9.4 ng m^{-3}) > MSA (5.4 ± 5.2 ng m^{-3}).
326 The relative order of abundance varies for the sub- and super-micrometer ranges with the only
327 consistent feature being that oxalate was the most abundant species. This result was consistent
328 with past works showing oxalate to be the most abundant organic acid in different global regions

9

329 (e.g., Decesari et al. (2006); Kerminen et al. (1999); Sorooshian et al. (2007b); Ziemba et al.
330 (2011)).

331 Figure 2 shows the combined contribution of the organic acids and MSA to total gravimetric
332 mass, while Table S5 summarizes percent contributions of individual species to total mass for
333 different size bins. Combined, the measured organic acids and MSA accounted for only a small
334 part of the total cumulative mass (0.80 ± 0.66 %) across the 11 individual gravimetric sets. When
335 the combined contribution of organic acids and MSA to total gravimetric mass were separated by
336 season, results are generally the same (Fig. S1), with differences in the percent range being as
337 follows: SWM18 = 0.64 %; Transitional = 0.95 %; NEM = 0.50 – 1.49 %; and SWM19 = 0.23 –
338 0.83 %. The highest contribution of these organic acids and MSA occurred for MOUDI sets
339 collected 12 – 14 March 2019 during the NEM season, which accounted for 1.49 % (0.50 μg m^{-3})
340 of the total mass. The lowest contribution of these organic acids and MSA occurred for MOUDI
341 sets collected 11 – 13 September 2019 during the SWM19 season, which accounted for 0.23 %
342 (0.06 μg m^{-3}) of the total mass. The summed contributions of the six species were nearly the
343 same in the sub- and supermicrometer ranges (0.78 ± 0.74 % and 0.84 ± 0.58 %, respectively).
344 Their contributions peaked in the two sizes bins covering the range between 0.56 and 1.8 μm
345 ($0.56 – 1$ μm: 1.06 ± 1.01 %; $1 – 1.8$ μm: 1.01 ± 0.78 %). After accounting for all measured
346 species (BC, water-soluble species), there still remained 33.74 ± 19.89 % (range: 23.86 – 50.88
347 %) of unresolved mass. Therefore, the six species of interest in this work only explain a small
348 amount of the region's mass concentrations and further work is still needed to resolve the
349 remaining components, which presumably is dominated by water-insoluble organics and
350 elements. Of most need is to resolve those missing components in the supermicrometer range,
351 where Table S5 shows that the unresolved fraction is 69.10 ± 25.91 %, in contrast to $17.78 \pm$
352 17.25 % for the submicrometer range.

353 Although there are fairly wide ranges in concentration for the individual species, a few features
354 are noteworthy based on the cumulative dataset. First, the oxalate concentrations are lower than
355 expected for such a highly polluted area, as will be expanded upon in Sect. 5.5. Second, there is a
356 significant decrease in concentration after oxalate for the remaining five species, which had
357 similar mean concentrations. Lastly, although the sampling site is on an island and close to
358 marine sources, MSA is surprisingly the least abundant among the six species of interest.

359 Mean mass concentrations of these species varied greatly by season as visually shown in Fig. 3a
360 and summarized numerically in Table 1. In contrast, Fig. 3b shows that the mass fractions of the
361 six species did not change much seasonally owing to the dominance of oxalate (37.67 – 472.82
362 ng m^{-3}), which accounted for between 69.1-87.3 % of the cumulative concentration of the six
363 species across the four seasons. Important features with regard to seasonal mass concentration
364 differences include the following: (i) maleate concentrations were much higher in the SWM18
365 and SWM19 seasons; (ii) the lowest overall concentrations of most species, besides oxalate and
366 succinate (lowest in SWM19), were observed in the NEM season; (iii) oxalate and phthalate
367 were the only species that peaked in the Transitional period, whereas the rest of the species
368 peaked in either SWM18 or SWM19; and (iv) succinate and phthalate were peculiarly much

369 more enhanced in SWM18 than SWM19, pointing to significant variability between consecutive
370 years.

371

372 4.3 Source apportionment

373 To help elucidate how different emissions sources impact the six species, PMF analysis was
374 conducted and yielded a solution with five source factors using year-round data (Fig. 4). The five
375 sources are as follows in decreasing order of their contribution to the total mass based on the sum
376 of species used in the PMF analysis (Fig. 4): combustion (32.1 %), biomass burning (20.9 %),
377 sea salt (20.9 %), crustal (14.2 %), and waste processing (11.9 %). The contribution of each
378 source to the total concentration of organic acids and MSA was as follows: combustion (33.5 %),
379 biomass burning (29.0 %), crustal (27.0 %), waste processing (9.8 %), and sea salt (0.6 %). The
380 source factor names were determined based on the enhancement of the following species (Fig.
381 4): (i) crustal (Al, Ti) (Harrison et al., 2011; Malm et al., 1994; Singh et al., 2002), (ii) biomass
382 burning (K, Rb) (Andreae, 1983; Artaxo et al., 1994; Braun et al., 2020; Chow et al., 2004;
383 Echalar et al., 1995; Ma et al., 2019; Schlosser et al., 2017; Thepnuan et al., 2019; Yamasoe et
384 al., 2000), (iii) sea salt (Na, Cl) (Seinfeld and Pandis, 2016), (iv) combustion (V, Ni, As) (Allen
385 et al., 2001; Linak et al., 2000; Mahowald et al., 2008; Mooibroek et al., 2011; Prabhakar et al.,
386 2014; Wasson et al., 2005), and (v) waste processing (Cd, Pb) (Cruz et al., 2019; Gullett et al.,
387 2007; Iijima et al., 2007; Pabroa et al., 2011). While both SO_4^{2-} and NO_3^- are secondarily
388 produced, the latter is more commonly linked to supermicrometer particles (Allen et al., 1996;
389 Dasgupta et al., 2007; Fitzgerald, 1991; Maudlin et al., 2015), including in the study region
390 (Cruz et al., 2019). Additionally, Al, K, and Cl are linked to biomass burning (Reid et al., 1998;
391 Reid et al., 2005; Schlosser et al., 2017; Wonaschütz et al., 2011). The source factor names
392 should be interpreted with caution, as a single profile may consist of a mix of sources (e.g., waste
393 processing). It should be noted that Cruz et al. (2019) performed PMF analysis for only the
394 SWM18 season, which yielded similar and additional sources for only the SWM18 season,
395 whereas this study used year-round data.

396 To provide size-resolved context for the five aerosol sources, Fig. 5 shows their respective
397 reconstructed mass size distributions based on PMF output. Distributions for combustion,
398 biomass burning, and waste processing primarily peaked in the submicrometer range, while
399 crustal and sea salt sources primarily peaked in the supermicrometer range. Combustion and
400 biomass burning factors showed a dominant peak between 0.32 – 0.56 µm, whereas waste
401 processing had a peak between 0.56 – 1 µm. The crustal and sea salt factors exhibited their peak
402 concentrations between 1.8 – 5.6 µm. Both crustal and biomass burning sources showed signs of
403 bimodal size distributions with a minor peak in the sub- and supermicrometer ranges,
404 respectively.

405 As reported in Table 2, combustion was the largest contributor to the cumulative mass
406 concentrations of organic acids and MSA, with the largest influence being for maleate (69.7 %)
407 and MSA (57.4 %). Biomass burning was marked by its significant contribution to succinate
408 (90.3 %). The sea salt source showed minor contributions to phthalate (9.9 %) and adipate (4.7

11

409   %). The crustal source contributed appreciably to adipate (35.9 %) and oxalate (31.2 %), with the
410   rest of the organic acid or MSA species being less influenced (0.1 – 13.3 %). Organic acids have
411   been shown in past work to be associated with mineral dust (Russell et al., 2002), including both
412   oxalic and adipic acids (Falkovich et al., 2004; Kawamura et al., 2013; Sullivan and Prather,
413   2007; Tsai et al., 2014), although less has been documented for adipate. Wang et al. (2017) and
414   Yao et al. (2003) both report that gaseous acids are likely to adsorb onto supermicrometer
415   particles that are highly alkaline, such as dust. The waste processing factor contributed to
416   maleate (30.1 %), oxalate (10.5 %), and MSA (1.4 %). An unexpected result was that the sea salt
417   factor did not contribute to MSA even though the latter is derived from ocean-emitted DMS; the
418   results of Table 2 suggest that other sources such as biomass burning and industrial activities are
419   more influential in the study region similar to other regions like Beijing (Yuan et al., 2004) and
420   coastal and inland areas of California (Sorooshian et al., 2015).

421

422   4.4 Species interrelationships

423   Correlation analysis was conducted for the same species used in the PMF analysis to quantify
424   interrelationships and to gain additional insight into common production pathways. Correlation
425   coefficients (r) values are reported in Table 3 for for the sub- and supermicrometer ranges,
426   whereas results for full size range are shown in Table S6. Values are only shown and discussed
427   subsequently for correlations with p-values below 0.05. Unless otherwise stated, correlations
428   discussed below correspond to the full size range for simplicity, whereas notable results when
429   contrasting the two size ranges (< 1 μm and > 1 μm) are explicitly mentioned.

430   MSA exhibited a statistically significant correlation with Rb (r = 0.37), suggestive of its link
431   with biomass burning as Rb has been shown in the study region to be a biomass burning marker
432   (Braun et al., 2020). Additionally, MSA was correlated with Na, NO_3^-, and SO_4^{2-} (r: 0.35 – 0.59),
433   which are associated with marine aerosol (e.g., sea salt, DMS, shipping) but also biomass
434   burning. The supermicrometer results indicate MSA was correlated only with Na (r = 0.32), due
435   presumably to co-emission from both crustal and sea salt sources, with the former commonly
436   linked to biomass burning (Schlosser et al., 2017). For the submicrometer range, MSA was
437   correlated with Rb and SO_4^{2-} (r: 0.39 – 0.60), which are derived from biomass burning and other
438   forms of combustion, consistent with smaller particles formed secondarily from gas-to-particle
439   conversion processes. That is also why MSA was well correlated with succinate, oxalate, and
440   phthalate (r: 0.53 – 0.67), which were also prominent species in either (or both of) the biomass
441   burning and combustion factors.

442   Adipate only exhibited significant correlations with maleate and phthalate for the full diameter
443   range (r: 0.43 – 0.45), while maleate was correlated only with adipate. In contrast, succinate,
444   oxalate, and phthalate were correlated with a wide suite of species, indicating that maleate and
445   adipate exhibited more unique behavior in terms of their production routes. Succinate, oxalate,
446   and phthalate similarly exhibited significant correlations with each other, and species linked to
447   crustal sources (Al, Ti, Na), sea salt (Na), and biomass burning (Rb). Succinate and oxalate in

448 particular were better correlated with tracer species related to either dust or sea salt (Al, Na) in
449 the supermicrometer range, and were correlated with each other also in that size range.

450

451 4.5 Cumulative size distribution variations

452 Mass size distributions for each individual organic acid and MSA are shown for the full study
453 period in Fig. S2 and seasonal mass size distributions can be seen in Figs. 6-11. General
454 information for the cumulative dataset will be described here before examining seasonal results
455 in Sect. 5. While significant variability exists between individual sets for the cumulative dataset,
456 a few general features are evident: (i) mass size distributions all appear multi-modal with the
457 exception of maleate, which on average exhibited a uni-modal profile; (ii) all species show a
458 larger peak in the submicrometer range versus supermicrometer sizes; (iii) phthalate and adipate
459 show more comparable peaks in the sub- and supermicrometer range; and (iv) the size bin where
460 the peaks occur vary between species. These results point to differences in the species with
461 regard to their source, formation mechanism, and eventual fate.

462 One factor relevant to the mass size distribution plots is the source origin of sampled air masses.
463 The CWT plots in Fig. 12 reveal the bulk of the concentration of a few species (e.g., phthalate,
464 succinate, and MSA) was explained by southwesterly flow. Consistent with the PMF results
465 showing that the biomass burning factor contributed the most to these three species, the
466 predominant fire sources were to the southwest of Luzon. Past work has linked these areas to
467 significant biomass burning influence over Luzon and the South China Sea during the SWM
468 season (Atwood et al., 2017; Ge et al., 2017; Hilario et al., 2020b; Reid et al., 2016; Song et al.,
469 2018; Wang et al., 2013; Xian et al., 2013). Noteworthy is that the CWT maps for SWM18
470 reveal more influence from the biomass burning hotspots to the southwest (e.g., Borneo and
471 Sumatra), in contrast to SWM19, pointing to more biomass burning influence in the former
472 season. Oxalate's CWT profile shows the most spatial heterogeneity in terms of source regions;
473 this is consistent with it being an end-product in the oxidation of other carboxylic acids that can
474 originate from numerous sources. Finally, adipate and maleate similarly showed a localized
475 hotspot in terms of where their greatest influence originated, approximately 290 km to the north-
476 northwest of MO. This could be partly linked to the Sual coal-fired power station located near
477 that area where an ash disposal site is also in close proximity. The uniquely similar CWT maps
478 between adipate and maleate is consistent with them having few correlations, if any, with species
479 aside from each other (Table S6). Subsequent sections discuss each organic acid and MSA in
480 more detail, beginning with larger acids since knowledge of their behavior is important to better
481 understand the smaller acids.

482

483 **5. Discussion**

484 5.1 Phthalate

485 Results from Sect. 4 show that phthalate has the following characteristics:

13

486   (i) influenced most by biomass burning (49.5 %), followed by combustion (27.4 %), crustal
487   sources (13.3 %), and then sea salt (9.9 %);

488   (ii) significant correlations with more species in Table S6 than any other organic acid or MSA;

489   (iii) comparable mass size distribution modes in the sub- and supermicrometer size ranges;

490   (iv) highest mass concentration in the Transitional period, but also exhibited significantly
491   different concentrations between the two SWM seasons;

492   (v) had concentrations dominated by sources to the southwest.

493   A more detailed examination based on seasonally resolved mass size distributions and CWT
494   maps follows to try to gain more insights into this species. Although not referenced hereafter,
495   Table S7 provides numerical details about mass concentration mode sizes and associated
496   concentrations for each season and the cumulative dataset for each species.

497   The average size distributions for phthalate appeared bi-modal for each individual season (Fig.
498   6). Depending on the season, concentration peaks occurred in three separate MOUDI stages for
499   the submicrometer range, and between 1.8 – 3.2 or 3.2 – 5.6 µm in the supermicrometer range.
500   The NEM season was unique in that the supermicrometer peak was considerably more
501   pronounced than in the submicrometer range, which was a rare occurrence in this study for all
502   species except adipate. Phthalate appears in the submicrometer range due to secondary formation
503   by photo-oxidation (i.e., Kautzman et al., 2010; Kawamura and Ikushima, 2002; Kawamura and
504   Yasui, 2005; Kleindienst et al., 2012) and from primary emissions (i.e., combustion,
505   biomass/waste burning) (i.e., Deshmukh et al., 2016; Kawamura and Kaplan, 1987; Kumar et al.,
506   2015; Kundu et al., 2010). Its general presence in the supermicrometer range, especially during
507   the NEM season, can be explained by possible adsorption onto larger particles such as dust and
508   sea salt (i.e., Wang et al., 2012; Wang et al., 2017). Others have observed an enhancement in
509   phthalate in the supermicrometer mode, specifically in Xi'an, China, due to suspected adsorption
510   of its vapor form (Wang et al., 2012) derived from photo-oxidation of naphthalene (Ho et al.,
511   2006; Wang et al., 2011; Wang et al., 2012; Wang et al., 2017).

512   CWT results for phthalate (Fig. S3) showed high concentrations across all seasons coming from
513   the southwest, most notably in the SWM18 and SWM19 seasons. The significant reduction in
514   phthalate levels from SWM18 (17 ± 25 ng m^{-3}) to SWM19 (5.7 ± 7.4 ng m^{-3}) is coincident with
515   stronger influence from biomass burning from the southwest in 2018. Figure 3 showed that the
516   highest concentration of phthalate occurred in the Transitional period, assumed to be largely due
517   to local emissions (e.g., vehicular traffic) based on the CWT results with significant influence in
518   the immediate vicinity of Luzon unlike the other seasons. The peculiar size distribution results
519   for the NEM season can be explained by the CWT map showing strong influence from the
520   northeast, which likely includes supermicrometer aerosol influences from sea salt and dust from
521   East Asia. The reduced influence of upwind anthropogenic and biomass burning emissions
522   during the NEM season can explain the lower seasonal concentrations, especially in the
523   submicrometer size range (Hsu et al., 2009).

524

525   5.2 Adipate

526   Adipate was shown in Sect. 4 to have the following features:

527   (i) influenced most by crustal sources (35.9 %), followed by combustion (32.9 %), biomass
528   burning (26.4 %), and finally sea salt (4.7 %);

529   (ii) only correlated with maleate and phthalate;

530   (iii) comparable concentrations in the sub- and supermicrometer size ranges, with a mode
531   between 5.6 and 10 μm;

532   (iv) highest mass concentration in the SWM seasons, but especially the SWM19 season;

533   (v) concentrations dominated by sources from the southwest as well as from the northwest.

534   Mass size distributions for adipate were the most variable in structure compared to the other five
535   species with multiple peaks present at different sizes (Fig. S2). In general, its distributions
536   appeared uniquely and consistently tri-modal with the exception of the SWM18 season where it
537   was bi-modal (Fig. 7). Modes appeared between 0.10 – 0.18 μm and 0.32 – 0.56 μm for the
538   submicrometer range, and between 1.0 – 1.8 μm and 3.2 – 5.6 μm in the supermicrometer range.
539   The SWM19 season was unique for adipate as the highest peak was in the supermicrometer
540   range and it was higher than any other peak across the other seasons. Submicrometer adipate is
541   likely derived from a photo-oxidation of higher chain organic acids (i.e., van Drooge and
542   Grimalt, 2015), ozonolysis of vehicular emissions (i.e., Grosjean et al., 1978), and from the
543   primary emissions of biomass burning (i.e., Graham et al., 2002). The appearance in the
544   supermicrometer range likely due to adsorption onto larger particles such as dust and sea salt
545   (e.g., Wang et al., 2012; Wang et al., 2017). As the PMF results suggest crustal sources were
546   more influential for adipate in contrast to sea salt, dust was more likely the supermicrometer
547   particle type that adipate preferentially partitioned to. The source of the dust was likely a
548   combination of long-range transport from (i) the southwest especially during biomass burning
549   periods, (ii) East Asia, and (iii) locally generated dust via anthropogenic activities (Fig. S4).

550   Past work in the study region showed that broad mass size distributions with comparable
551   concentrations in the sub- and supermicrometer ranges were coincident with wet scavenging
552   (Braun et al., 2020) and appreciable primary emissions of sea salt and dust (AzadiAghdam et al.,
553   2019; Cruz et al., 2019). Scavenging was suggested to remove transported pollution while
554   allowing for more pronounced contributions from more localized emissions, which could include
555   vehicular traffic, sea salt, and anthropogenic forms of dust (e.g., road dust, construction), all of
556   which are consistent with adipate's mass size distribution data and CWT maps (Fig. S4) showing
557   high concentrations predominately around Luzon for all seasons.

558

559   5.3 Succinate

560   Succinate exhibited the following characteristics:

15

561   (i) influenced primarily by biomass burning (90.3 %) followed by crustal sources (9.7 %);

562   (ii) exhibited high correlation coefficients (0.67 – 0.76) with oxalate, phthalate, and MSA (Table
563   S6);

564   (iii) mass was focused in the submicrometer range;

565   (iv) highest mass concentrations were in the SWM18 season, and, similar to phthalate, showed a
566   significant reduction in the SWM19 season;

567   (v) had concentrations dominated by sources from the southwest.

568   The average size distributions for succinate varied in the number of peaks present (2 – 4), but on
569   average were bi-modal with a submicrometer mode usually between 0.32 – 0.56 μm or 0.56 – 1.0
570   μm, and a smaller supermicrometer mode between either 1.8 – 3.2 μm or 3.2 – 5.6 μm (Fig. 8).
571   The chief source of succinate, which is concentrated in the submicrometer peak, is biomass
572   burning (Pratt et al., 2011; Vasconcellos et al., 2010), which is reinforced by the PMF results
573   (Table 2), its high correlation with the biomass burning tracer Rb (r = 0.67; Table S6) (Braun et
574   al., 2020) and CWT maps showing its most pronounced influence from biomass burning hotspots
575   to the southwest during the SWM18 season (Fig. S5). There likely was also local biomass
576   burning during the NEM season contributing to succinate concentrations. Hilario et al. (2020a)
577   showed based on satellite data that local fire activity peaks between March and May. There was
578   less influence from biomass burning in the SWM19 season, which is why succinate's levels were
579   lower (4.7 ± 7.4 ng m^{-3}) than in the SWM18 season (22 ± 43 ng m^{-3}). Similar to phthalate and
580   adipate, there were more local hotspots of concentration in seasonal CWT maps pointing to local
581   anthropogenic sources such as vehicular traffic and the presence of supermicrometer particles
582   like dust and sea salt that succinate can partition to (e.g., Wang et al., 2012; Wang et al., 2017).

583

584   5.4 Maleate

585   The results of Sect. 4 showed that maleate had the following attributes:

586   (i) influenced most by combustion (69.7 %), followed by waste processing (30.1 %), and then
587   barely by crustal sources (0.2 %);

588   (ii) only correlated with adipate of all species shown in Table S6;

589   (iii) showed a uni-modal mass size distribution, with negligible contribution in the
590   supermicrometer range;

591   (iv) highest mass concentration in the SWM19 season, but was comparable to the SWM18
592   season;

593   (v) CWT maps showed the most localized sources as compared to the other species examined
594   (Fig. 11).

595 The average seasonal size distributions for maleate appeared to be uni-modal with peaks between
596 0.32 – 0.56 µm and 0.56 – 1.0 µm (Fig. 9). The absence of a supermicrometer peak, in contrast to
597 most other species, suggests that it had less diverse sources and was derived from combustion
598 emissions without being adsorbed onto supermicrometer particles like the other species
599 investigated. The association of maleate with the waste processing source factor in Table 2 can
600 be explained partly by the burning and recycling of electronic waste (Cruz et al., 2019; Gullett et
601 al., 2007; Iijima et al., 2007). The Pabroa et al. (2011) study reported that there are few licensed
602 operators for battery recycling, but there are numerous unregulated melters frequently melting
603 metal and discarding the waste.

604 Seasonal CWT maps for maleate (Fig. S6) consistently showed hotspots around Luzon indicative
605 of local emissions. Maleate concentrations for the SWM18 (19 ± 15 ng m^{-3}) and SWM19 (19 ±
606 34 ng m^{-3}) were significantly higher than the other seasons (Transitional: 3.8 ± 4.2 ng m^{-3}; NEM:
607 1.7 ± 3.7 ng m^{-3}), and this could likely be due to increased traffic emissions because of gridlock
608 due to intense rainfall. It should be noted that the Ateneo de Manila campus has student break
609 periods in March, April, May, and December (Hilario et al., 2020a); those months pertain to the
610 NEM season, which could lead to lower combustion emissions from vehicles (e.g., maleate and
611 phthalate). Although the SWM season is associated with enhanced precipitation over Metro
612 Manila, lower boundary layer height and appreciable RH values could counteract wet scavenging
613 to some degree by promoting aqueous processing of aerosol (Hilario et al., 2020a). Furthermore,
614 maleate's largely submicrometer size distribution (Fig. 9) may reduce the efficiency of wet
615 scavenging (Greenfield, 1957).

616

617 5.5 Oxalate

618 Oxalate was shown to have the following traits:

619 (i) influenced somewhat uniformly by combustion (32.9 %) and crustal (31.2 %) sources,
620 followed by biomass burning (25.4 %), and waste processing (10.5 %);

621 (ii) only organic acid to correlate with combustion tracers (V, Ni);

622 (iii) pronounced presence in both the sub- and supermicrometer size ranges;

623 (iv) highest mass concentrations in the Transitional period;

624 (v) had contributions from the southwest, east/northeast, and locally.

625 Oxalate concentrations in this study (37.67 – 472.82 ng m^{-3}) were surprisingly low for such a
626 polluted megacity with strong regional sources. For context, concentrations in a few other
627 regions are as follows: 270 – 1,350 ng m^{-3} in Tokyo, Japan (Kawamura and Ikushima, 2002;
628 Sempére and Kawamura, 1994); 195 – 669 ng m^{-3} in Beijing, China (Du et al., 2014); and 149 –
629 735 ng m^{-3} in Thumba, India (Hegde et al., 2016).

630 The average size distributions for oxalate appeared bi-modal for each individual season with
631 modes between 0.32 – 0.56 µm and 0.56 – 1.0 µm for the submicrometer range and a separate

632   mode between 1.8 – 3.2 μm for the supermicrometer range (Fig. 10). A unique aspect for oxalate
633   was its consistency in having a bi-modal profile each season with the supermicrometer mode
634   always between 1.8 – 3.2 μm. Note that the modes discussed here represent the most pronounced
635   ones but others could have been present too reflecting other sources. Submicrometer oxalate
636   likely originated from secondary production from both biogenic and anthropogenic precursor
637   emissions, and potentially from primary emissions (i.e., combustion/biomass burning) (i.e.,
638   Decesari et al., 2006; Falkovich et al., 2005; Golly et al., 2019; Kundu et al., 2010; Wang et al.,
639   2010). Of all the six species studied, oxalate was best correlated with SO_4^{2-} (r = 0.69; Table S6),
640   especially in the submicrometer range (r = 0.72; Table 3), which is consistent with their common
641   production mechanism via aqueous processing (Sorooshian et al., 2006; Yu et al., 2005).
642   Additionally, high concentrations of oxalate in the Transitional period suggest that photo-
643   oxidation was an important process for oxalate formation since the Transitional period had low
644   rain and high solar radiation. The prominent supermicrometer presence was likely due to
645   adsorption onto supermicrometer particles. Past work by Sullivan and Prather (2007) reported
646   the following with regard to oxalate's behavior in coarse particles of relevance to this study: (i)
647   oxalic acid was predominately associated with mineral dust and to a lesser degree with aged sea
648   salt; (ii) even though most of the total mass was sea salt, there was more oxalate per mass of
649   mineral dust than sea salt; (iii) Asian dust particles are more alkaline as opposed to sea salt and
650   therefore act as better sinks for dicarboxylic acids than sea salt; and (iv) it is feasible that a large
651   fraction of supermicrometer dicarboxylic acid mass in remote marine air is associated with
652   mineral dust and not sea salt. The PMF results from the present study suggest that oxalate was
653   much more influenced by crustal sources (31.2 %) versus sea salt (0 %), similar to phthalate,
654   adipate, and succinate (Table 2). Reinforcing the relationship between oxalate and dust is the
655   significant correlation between oxalate and both Al (r = 0.59) and Ti (0.29) in the
656   supermicrometer range.

657   CWT results for oxalate (Fig. S7) showed high concentrations around Luzon for all seasons, with
658   the caveat that the SWM18 exhibited high concentrations coming from the southwest, which has
659   already been linked to biomass burning emissions. The difference in oxalate levels between the
660   SWM18 (178 ± 139 ng m^{-3}) and SWM19 (110 ± 62 ng m^{-3}) seasons is largely due to the
661   enhanced contribution of biomass burning in the former season since oxalate is abundant in fire
662   emissions (Falkovich et al., 2005; Mardi et al., 2018; Narukawa et al., 1999).

663

664   5.6 MSA

665   Previous sections revealed the following characteristics for MSA:

666   (i) influenced most by combustion (57.4 %), followed by biomass burning (41.2 %), waste
667   processing (1.4 %), and then crustal sources (0.1 %);

668   (ii) significantly correlated with succinate, oxalate, phthalate, and SO_4^{2-};

669   (iii) similar to maleate, primarily consisted of a submicrometer mass size distribution peak with
670   only minor contributions from the supermicrometer mode;

671   (iv) concentration was highest during the SWM18 season;

672   (v) had concentrations dominated by sources from the southwest.

673   Concentrations of MSA in this study were surprisingly low for a site so close to marine and
674   anthropogenic sources ($0.10 – 23.23$ ng m^{-3}). For context, MSA concentrations in nearby regions
675   are as follows: $30 – 60$ ng m^{-3} in Nanjing, China (Yang et al., 2005); $29 – 66$ ng m^{-3} over the
676   China Sea (Gao et al., 1996).

677   The average size distributions for MSA appeared uni-modal with the peak size being between
678   $0.32 – 0.56$ μm (Fig. 11). The consistent mass size distribution for MSA in all seasons, similar to
679   maleate, could be due to some combination of limited sources and production pathways.
680   Surprisingly, MSA showed no association to the sea salt source factor (Table 2) even though it
681   would be expected given that DMS is co-emitted from the ocean with sea salt. Due to the
682   proximity of the sampling site to the ocean it is possible that the local sea salt was relatively
683   fresh with short transport time, which could potentially explain the lack of an association with
684   MSA as it requires time to be produced from its marine precursor DMS. Instead, combustion and
685   biomass burning sources were more significantly related to MSA, which is consistent with some
686   past studies linking MSA to anthropogenic sources (Yuan et al., 2004) and biomass burning
687   (Sorooshian et al., 2015). Consequently, concentrations of MSA from these other non-marine
688   sources could be much higher causing the PMF model to associate MSA with non-sea salt
689   related sources. CWT results for MSA (Fig. S8) showed high concentrations coming from the
690   southwest during the SWM18 and SWM19 seasons, and from the east-northeast during the NEM
691   and Transitional period.

692   Both MSA and oxalate had significantly lower concentrations than other regions, and there are a
693   few possible explanations for this. First, it is worth noting that degradation of these species is
694   unlikely due to storage or sonication as careful procedures were followed as noted in Sect. 2.2.
695   The Philippines has relatively high temperatures, humidity, and solar radiation year-round,
696   providing optimal conditions for processing and degradation to occur, yielding low
697   concentrations for MSA and oxalate. Furthermore, there are mechanisms by which species such
698   as oxalate can be degraded via complexation effects with metal cations (Paris and Desboeufs,
699   2013; Siffert and Sulzberger, 1991; Sorooshian et al., 2013; Zuo, 1995), which are abundant in
700   the study region.

701

702   **6. Conclusions**

703   This work used a 16-month long dataset of size-resolved aerosol composition to investigate the
704   nature of five organic acids (oxalate, succinate, adipate, maleate, and phthalate) and MSA in the
705   polluted Metro Manila region in the Philippines. Selected results are as follows in order of the
706   three major questions posed at the end of Sect. 1.

707   • Organic acids and MSA contribute only a small fraction to the total gravimetric aerosol
708   mass in Metro Manila (0.80 ± 0.66 %). The combined contribution of these six species
709   was similar between the sub- and supermicrometer range (0.78 % and 0.84 %,

710	respectively). After accounting for water-soluble ions and elements, and black carbon,
711	there still was an unresolved mass fraction amounting to 33.74 % across all sizes, and
712	17.78 % and 69.10 % for sub- and supermicrometer sizes, respectively. Therefore, future
713	work is still warranted to identify what the missing fraction is comprised of, which is
714	speculated to be water-insoluble organics and elements.
715	• Oxalate was the most abundant of the six species accounting for 69.1 – 87.3 % of the
716	total combined mass of the six species depending on the season. However, the bulk
717	concentrations of oxalate were unusually low (149 ± 94 ng m^{-3}) for such a polluted area
718	in contrast to other populated regions. Concentrations of the other five species were much
719	lower than oxalate, with mean levels for the entire study period being less than 10 ng m^{-3}.
720	In particular, MSA exhibited the lowest mean concentration (5.4 ± 5.2 ng m^{-3}). It is
721	unclear exactly as to the reason for the low concentrations of the examined species in
722	light of the diverse marine and anthropogenic sources in the region. The role of wet
723	scavenging, especially in the SWM seasons, will be the subject of future research.
724	• The six species exhibited different behavior seasonally, both in terms of relative
725	concentration and mass size distribution. The SWM18 season was uniquely different than
726	the SWM19 season, owing to more biomass burning emissions transported from the
727	southwest that yielded enhanced levels for most species in the submicrometer range,
728	especially succinate, MSA, oxalate, and phthalate. Enhanced precipitation in the SWM
729	seasons also was coincident with more influence from localized emissions leading to
730	enhanced levels in the sub- and supermicrometer ranges depending on the species. The
731	NEM season was characterized by generally lower concentrations of most species as air
732	was predominantly transported from the northeast with reduced influence of
733	anthropogenic and biomass burning emissions. Phthalate was enhanced in the
734	supermicrometer range during the NEM season due to presumed adsorption to Asian dust
735	and to a lesser extent sea salt. The Transitional season was characterized by having strong
736	influence from localized emissions for all six species, which promoted especially high
737	concentrations for phthalate and oxalate in both the sub- and supermicrometer ranges.
738	• All species exhibited a prominent submicrometer peak that likely stemmed largely from
739	secondary formation from both anthropogenic and biogenic precursor emissions and was
740	especially prominent during the SWM18 season due to extensive biomass burning
741	influence. Biomass burning was an especially important source for succinate, phthalate,
742	MSA, oxalate, and adipate. All six species exhibited relatively low association with sea
743	salt particles; this was particularly interesting for MSA, which was instead better related
744	to combustion and biomass burning emissions. In contrast to sea salt, most species were
745	linked to crustal emissions as evident from peaks in the coarse mode during periods of
746	dust influence. Oxalate, adipate, phthalate, and succinate in particular preferentially
747	partitioned to dust rather than sea salt, potentially due to their affinity for alkaline particle
748	types. Oxalate was best correlated with sulfate, especially in the submicrometer mode,
749	explained by their common production via aqueous processing, which is common in the
750	study region owing to high humidity levels year-round.

The results of this study point to the importance of size-resolved measurements of organic and sulfonic acids as this extensive dataset revealed important changes in mass size distributions between species and for different seasons. The data point to the partitioning of these species to coarse aerosol types and the potentially significant impact of precipitation on either the removal or enhancement of species' mass size distribution modes; these topics warrant additional research to put on firmer ground the sensitivity of these species to source regions, transport pathway, and wet scavenging effects. More research is warranted to investigate the remaining fraction of the unresolved mass (approximately one third of the gravimetric mass) that is not accounted for by black carbon and the water-soluble constituents speciated in this work. This is especially important for the supermicrometer range. Lastly, the current results point to the question as to what drives the affinity of individual species towards the coarse mode for different aerosol types (e.g., dust, sea salt), and how common this is for other regions.

Data availability

Size-resolved aerosol data collected at Manila Observatory are described in Stahl et al. (2020a) and archived on figshare (Stahl et al., 2020b) as well as on the NASA data repository at DOI:10.5067/Suborbital/CAMP2EX2018/DATA001.

Author contribution

MTC, MOC, JBS, RAB, ABM, CS, and AS designed the experiment. All coauthors carried out various aspects of the data collection. MTC, RAB, CS, and AS conducted analysis and interpretation of the data. CS and AS prepared the manuscript with contributions from the coauthors.

Competing interests

The authors declare that they have no conflict of interest.

References

787   Adam, M. G., Chiang, A. W. J., and Balasubramanian, R.: Insights into characteristics of light
788   absorbing carbonaceous aerosols over an urban location in Southeast Asia, Environ Pollut, 257,
789   113425, 10.1016/j.envpol.2019.113425, 2020.
790   Agarwal, R., Shukla, K., Kumar, S., Aggarwal, S. G., and Kawamura, K.: Chemical composition
791   of waste burning organic aerosols at landfill and urban sites in Delhi, Atmos Pollut Res, 11, 554-
792   565, 10.1016/j.apr.2019.12.004, 2020.
793   Akasaka, I., Morishima, W., and Mikami, T.: Seasonal march and its spatial difference of rainfall
794   in the Philippines, Int J Climatol, 27, 715-725, 10.1002/joc.1428, 2007.
795   Alas, H. D., Müller, T., Birmili, W., Kecorius, S., Cambaliza, M. O., Simpas, J. B. B., Cayetano,
796   M., Weinhold, K., Vallar, E., Galvez, M. C., and Wiedensohler, A.: Spatial Characterization of
797   Black Carbon Mass Concentration in the Atmosphere of a Southeast Asian Megacity: An Air
798   Quality Case Study for Metro Manila, Philippines, Aerosol Air Qual Res, 18, 2301-2317,
799   10.4209/aaqr.2017.08.0281, 2018.
800   Allen, A. G., Nemitz, E., Shi, J. P., Harrison, R. M., and Greenwood, J. C.: Size distributions of
801   trace metals in atmospheric aerosols in the United Kingdom, Atmos Environ, 35, 4581-4591,
802   10.1016/s1352-2310(01)00190-x, 2001.
803   Allen, H. C., Laux, J. M., Vogt, R., Finlayson-Pitts, B. J., and Hemminger, J. C.: Water-Induced
804   Reorganization of Ultrathin Nitrate Films on NaCl: Implications for the Tropospheric Chemistry
805   of Sea Salt Particles, J Phys Chem, 100, 6371-6375, 10.1021/jp953675a, 1996.
806   Andreae, M. O.: Soot carbon and excess fine potassium: long-range transport of combustion-
807   derived aerosols, Science, 220, 1148-1151, 10.1126/science.220.4602.1148, 1983.
808   Andreae, M. O., and Crutzen, P. J.: Atmospheric Aerosols: Biogeochemical Sources and Role in
809   Atmospheric Chemistry, Science, 276, 1052-1058, 10.1126/science.276.5315.1052, 1997.
810   Artaxo, P., Gerab, F., Yamasoe, M. A., and Martins, J. V.: Fine mode aerosol composition at
811   three long-term atmospheric monitoring sites in the Amazon Basin, J Geophys Res, 99, 22857-
812   22868, 10.1029/94jd01023, 1994.
813   Asmi, E., Frey, A., Virkkula, A., Ehn, M., Manninen, H. E., Timonen, H., Tolonen-Kivimäki, O.,
814   Aurela, M., Hillamo, R., and Kulmala, M.: Hygroscopicity and chemical composition of
815   Antarctic sub-micrometre aerosol particles and observations of new particle formation, Atmos
816   Chem Phys, 10, 4253-4271, 10.5194/acp-10-4253-2010, 2010.
817   Atwood, S. A., Reid, J. S., Kreidenweis, S. M., Blake, D. R., Jonsson, H. H., Lagrosas, N. D.,
818   Xian, P., Reid, E. A., Sessions, W. R., and Simpas, J. B.: Size-resolved aerosol and cloud
819   condensation nuclei (CCN) properties in the remote marine South China Sea – Part 1:
820   Observations and source classification, Atmos Chem Phys, 17, 1105-1123, 10.5194/acp-17-
821   1105-2017, 2017.
822   AzadiAghdam, M., Braun, R. A., Edwards, E.-L., Bañaga, P. A., Cruz, M. T., Betito, G.,
823   Cambaliza, M. O., Dadashazar, H., Lorenzo, G. R., Ma, L., MacDonald, A. B., Nguyen, P.,
824   Simpas, J. B., Stahl, C., and Sorooshian, A.: On the nature of sea salt aerosol at a coastal
825   megacity: Insights from Manila, Philippines in Southeast Asia, Atmos Environ, 216, 116922,
826   10.1016/j.atmosenv.2019.116922, 2019.
827   Baboukas, E. D., Kanakidou, M., and Mihalopoulos, N.: Carboxylic acids in gas and particulate
828   phase above the Atlantic Ocean, J Geophys Res-Atmos, 105, 14459-14471,
829   10.1029/1999jd900977, 2000.
830   Bagtasa, G., Cayetano, M. G., and Yuan, C.-S.: Seasonal variation and chemical characterization
831   of PM2.5 in northwestern Philippines, Atmos Chem Phys, 18, 4965-4980, 10.5194/acp-18-4965-
832   2018, 2018.

833 Bagtasa, G., Cayetano, M. G., Yuan, C.-S., Uchino, O., Sakai, T., Izumi, T., Morino, I., Nagai,
834 T., Macatangay, R. C., and Velazco, V. A.: Long-range transport of aerosols from East and
835 Southeast Asia to northern Philippines and its direct radiative forcing effect, Atmos Environ,
836 218, 117007, 10.1016/j.atmosenv.2019.117007, 2019.
837 Bagtasa, G., and Yuan, C.-S.: Influence of local meteorology on the chemical characteristics of
838 fine particulates in Metropolitan Manila in the Philippines, Atmos Pollut Res, 11, 1359-1369,
839 10.1016/j.apr.2020.05.013, 2020.
840 Bañares, E. N., Narisma, G. T. T., Simpas, J. B. B., Cruz, F. A. T., Lorenzo, G. R. H.,
841 Cambaliza, M. O., and Coronel, R. C.: Diurnal characterization of localized convective rain
842 events in urban Metro Manila, Philippines, AGUFM, 2018, A11J-2367, 2018.
843 Barbaro, E., Padoan, S., Kirchgeorg, T., Zangrando, R., Toscano, G., Barbante, C., and
844 Gambaro, A.: Particle size distribution of inorganic and organic ions in coastal and inland
845 Antarctic aerosol, Environ Sci Pollut Res Int, 24, 2724-2733, 10.1007/s11356-016-8042-x, 2017.
846 Bardouki, H., Berresheim, H., Vrekoussis, M., Sciare, J., Kouvarakis, G., Oikonomou, K.,
847 Schneider, J., and Mihalopoulos, N.: Gaseous (DMS, MSA, SO2, H2SO4 and DMSO) and
848 particulate (sulfate and methanesulfonate) sulfur species over the northeastern coast of Crete,
849 Atmos Chem Phys, 3, 1871-1886, 10.5194/acp-3-1871-2003, 2003a.
850 Bardouki, H., Liakakou, H., Economou, C., Sciare, J., Smolík, J., Ždímal, V., Eleftheriadis, K.,
851 Lazaridis, M., Dye, C., and Mihalopoulos, N.: Chemical composition of size-resolved
852 atmospheric aerosols in the eastern Mediterranean during summer and winter, Atmos Environ,
853 37, 195-208, 10.1016/s1352-2310(02)00859-2, 2003b.
854 Bates, T. S., Lamb, B. K., Guenther, A., Dignon, J., and Stoiber, R. E.: Sulfur emissions to the
855 atmosphere from natural sources, J Atmos Chem, 14, 315-337, 10.1007/bf00115242, 2004.
856 Bautista, A. T., Pabroa, P. C. B., Santos, F. L., Racho, J. M. D., and Quirit, L. L.: Carbonaceous
857 particulate matter characterization in an urban and a rural site in the Philippines, Atmos Pollut
858 Res, 5, 245-252, 10.5094/apr.2014.030, 2014.
859 Beaver, M. R., Garland, R. M., Hasenkopf, C. A., Baynard, T., Ravishankara, A. R., and Tolbert,
860 M. A.: A laboratory investigation of the relative humidity dependence of light extinction by
861 organic compounds from lignin combustion, Environ Res Lett, 3, 045003, 10.1088/1748-
862 9326/3/4/045003, 2008.
863 Berresheim, H.: Biogenic sulfur emissions from the Subantarctic and Antarctic Oceans, J
864 Geophys Res, 92, 13245-13262, 10.1029/JD092iD11p13245, 1987.
865 Bikkina, S., Kawamura, K., Miyazaki, Y., and Fu, P.: High abundances of oxalic, azelaic, and
866 glyoxylic acids and methylglyoxal in the open ocean with high biological activity: Implication
867 for secondary OA formation from isoprene, Geophys Res Lett, 41, 3649-3657,
868 10.1002/2014gl059913, 2014.
869 Biona, J. B., Mejia, A., Tacderas, M., Cruz, N. D., Dematera, K., and Romero, J.: Alternative
870 Technologies for the Philippine Utility Jeepney A COST-BENEFIT STUDY, 2017.
871 Blando, J. D., and Turpin, B. J.: Secondary organic aerosol formation in cloud and fog droplets:
872 a literature evaluation of plausibility, Atmos Environ, 34, 1623-1632, 10.1016/s1352-
873 2310(99)00392-1, 2000.
874 Braun, R. A., Aghdam, M. A., Bañaga, P. A., Betito, G., Cambaliza, M. O., Cruz, M. T.,
875 Lorenzo, G. R., MacDonald, A. B., Simpas, J. B., Stahl, C., and Sorooshian, A.: Long-range
876 aerosol transport and impacts on size-resolved aerosol composition in Metro Manila, Philippines,
877 Atmos Chem Phys, 20, 2387-2405, 10.5194/acp-20-2387-2020, 2020.

878   Brown, S. G., Eberly, S., Paatero, P., and Norris, G. A.: Methods for estimating uncertainty in
879   PMF solutions: examples with ambient air and water quality data and guidance on reporting
880   PMF results, Sci Total Environ, 518-519, 626-635, 10.1016/j.scitotenv.2015.01.022, 2015.
881   Cai, C., Marsh, A., Zhang, Y. H., and Reid, J. P.: Group Contribution Approach To Predict the
882   Refractive Index of Pure Organic Components in Ambient Organic Aerosol, Environ Sci
883   Technol, 51, 9683-9690, 10.1021/acs.est.7b01756, 2017.
884   Carlton, A. G., Turpin, B. J., Lim, H.-J., Altieri, K. E., and Seitzinger, S.: Link between isoprene
885   and secondary organic aerosol (SOA): Pyruvic acid oxidation yields low volatility organic acids
886   in clouds, Geophys Res Lett, 33, 10.1029/2005gl025374, 2006.
887   Chebbi, A., and Carlier, P.: Carboxylic acids in the troposphere, occurrence, sources, and sinks:
888   A review, Atmos Environ, 30, 4233-4249, 10.1016/1352-2310(96)00102-1, 1996.
889   Chow, J. C., Watson, J. G., Kuhns, H., Etyemezian, V., Lowenthal, D. H., Crow, D., Kohl, S. D.,
890   Engelbrecht, J. P., and Green, M. C.: Source profiles for industrial, mobile, and area sources in
891   the Big Bend Regional Aerosol Visibility and Observational study, Chemosphere, 54, 185-208,
892   10.1016/j.chemosphere.2003.07.004, 2004.
893   Claeys, M., Vermeylen, R., Yasmeen, F., Gómez-González, Y., Chi, X., Maenhaut, W.,
894   Mészáros, T., and Salma, I.: Chemical characterisation of humic-like substances from urban,
895   rural and tropical biomass burning environments using liquid chromatography with UV/vis
896   photodiode array detection and electrospray ionisation mass spectrometry, Environ Chem, 9,
897   273-284, 10.1071/en11163, 2012.
898   Cohen, D. D., Stelcer, E., Santos, F. L., Prior, M., Thompson, C., and Pabroa, P. C. B.:
899   Fingerprinting and source apportionment of fine particle pollution in Manila by IBA and PMF
900   techniques: A 7-year study, X-Ray Spectrom, 38, 18-25, 10.1002/xrs.1112, 2009.
901   Crosbie, E., Sorooshian, A., Monfared, N. A., Shingler, T., and Esmaili, O.: A multi-year aerosol
902   characterization for the greater Tehran area using satellite, surface, and modeling data,
903   Atmosphere, 5, 178-197, 10.3390/atmos5020178, 2014.
904   Cruz, F. T., Narisma, G. T., Villafuerte, M. Q., Cheng Chua, K. U., and Olaguera, L. M.: A
905   climatological analysis of the southwest monsoon rainfall in the Philippines, Atmos Res, 122,
906   609-616, 10.1016/j.atmosres.2012.06.010, 2013.
907   Cruz, M. T., Bañaga, P. A., Betito, G., Braun, R. A., Stahl, C., Aghdam, M. A., Cambaliza, M.
908   O., Dadashazar, H., Hilario, M. R., Lorenzo, G. R., Ma, L., MacDonald, A. B., Pabroa, P. C.,
909   Yee, J. R., Simpas, J. B., and Sorooshian, A.: Size-resolved composition and morphology of
910   particulate matter during the southwest monsoon in Metro Manila, Philippines, Atmos Chem
911   Phys, 19, 10675-10696, 10.5194/acp-19-10675-2019, 2019.
912   Dasgupta, P. K., Campbell, S. W., Al-Horr, R. S., Ullah, S. M. R., Li, J., Amalfitano, C., and
913   Poor, N. D.: Conversion of sea salt aerosol to $NaNO_3$ and the production of HCl: Analysis of
914   temporal behavior of aerosol chloride/nitrate and gaseous HCl/HNO_3 concentrations with AIM,
915   Atmos Environ, 41, 4242-4257, 10.1016/j.atmosenv.2006.09.054, 2007.
916   Davis, D., Chen, G., Kasibhatla, P., Jefferson, A., Tanner, D., Eisele, F., Lenschow, D., Neff,
917   W., and Berresheim, H.: DMS oxidation in the Antarctic marine boundary layer: Comparison of
918   model simulations and held observations of DMS, DMSO, DMSO2, H_2SO_4(g), MSA(g), and
919   MSA(p), J Geophys Res-Atmos, 103, 1657-1678, 10.1029/97jd03452, 1998.
920   Dawson, M. L., Varner, M. E., Perraud, V., Ezell, M. J., Gerber, R. B., and Finlayson-Pitts, B. J.:
921   Simplified mechanism for new particle formation from methanesulfonic acid, amines, and water
922   via experiments and ab initio calculations, Proc Natl Acad Sci U S A, 109, 18719-18724,
923   10.1073/pnas.1211878109, 2012.

De Bruyn, W. J., Shorter, J. A., Davidovits, P., Worsnop, D. R., Zahniser, M. S., and Kolb, C. E.: Uptake of gas phase sulfur species methanesulfonic acid, dimethylsulfoxide, and dimethyl sulfone by aqueous surfaces, J Geophys Res, 99, 16927-16932, 10.1029/94jd00684, 1994.

Decesari, S., Fuzzi, S., Facchini, M. C., Mircea, M., Emblico, L., Cavalli, F., Maenhaut, W., Chi, X., Schkolnik, G., Falkovich, A., Rudich, Y., Claeys, M., Pashynska, V., Vas, G., Kourtchev, I., Vermeylen, R., Hoffer, A., Andreae, M. O., Tagliavini, E., Moretti, F., and Artaxo, P.: Characterization of the organic composition of aerosols from Rondônia, Brazil, during the LBA-SMOCC 2002 experiment and its representation through model compounds, Atmos Chem Phys, 6, 375-402, 10.5194/acp-6-375-2006, 2006.

Deshmukh, D. K., Kawamura, K., Lazaar, M., Kunwar, B., and Boreddy, S. K. R.: Dicarboxylic acids, oxoacids, benzoic acid, α-dicarbonyls, WSOC, OC, and ions in spring aerosols from Okinawa Island in the western North Pacific Rim: size distributions and formation processes, Atmos Chem Phys, 16, 5263-5282, 10.5194/acp-16-5263-2016, 2016.

Dimitriou, K.: The dependence of PM size distribution from meteorology and local-regional contributions, in Valencia (Spain)-A CWT model approach, Aerosol Air Qual Res, 15, 1979-1989, 10.4209/aaqr.2015.03.0162, 2015.

Dimitriou, K., Remoundaki, E., Mantas, E., and Kassomenos, P.: Spatial distribution of source areas of PM2.5 by Concentration Weighted Trajectory (CWT) model applied in PM2.5 concentration and composition data, Atmos Environ, 116, 138-145, 10.1016/j.atmosenv.2015.06.021, 2015.

Ding, X. X., Kong, L. D., Du, C. T., Zhanzakova, A., Fu, H. B., Tang, X. F., Wang, L., Yang, X., Chen, J. M., and Cheng, T. T.: Characteristics of size-resolved atmospheric inorganic and carbonaceous aerosols in urban Shanghai, Atmos Environ, 167, 625-641, 10.1016/j.atmosenv.2017.08.043, 2017.

Drozd, G., Woo, J., Häkkinen, S. A. K., Nenes, A., and McNeill, V. F.: Inorganic salts interact with oxalic acid in submicron particles to form material with low hygroscopicity and volatility, Atmos Chem Phys, 14, 5205-5215, 10.5194/acp-14-5205-2014, 2014.

Du, Z., He, K., Cheng, Y., Duan, F., Ma, Y., Liu, J., Zhang, X., Zheng, M., and Weber, R.: A yearlong study of water-soluble organic carbon in Beijing I: Sources and its primary vs. secondary nature, Atmospheric Environment, 92, 514-521, 2014.

Echalar, F., Gaudichet, A., Cachier, H., and Artaxo, P.: Aerosol emissions by tropical forest and savanna biomass burning: Characteristic trace elements and fluxes, Geophys Res Lett, 22, 3039-3042, 10.1029/95gl03170, 1995.

Ervens, B., Feingold, G., Clegg, S. L., and Kreidenweis, S. M.: A modeling study of aqueous production of dicarboxylic acids: 2. Implications for cloud microphysics, J Geophys Res, 109, 10.1029/2004jd004575, 2004.

Ervens, B., Sorooshian, A., Lim, Y. B., and Turpin, B. J.: Key parameters controlling OH-initiated formation of secondary organic aerosol in the aqueous phase (aqSOA), J Geophys Res-Atmos, 119, 3997-4016, 10.1002/2013jd021021, 2014.

Ervens, B.: Progress and Problems in Modeling Chemical Processing in Cloud Droplets and Wet Aerosol Particles, in: Multiphase Environmental Chemistry in the Atmosphere, ACS Symposium Series, ACS Publications, 327-345, 2018.

Falkovich, A. H., Schkolnik, G., Ganor, E., and Rudich, Y.: Adsorption of organic compounds pertinent to urban environments onto mineral dust particles, J Geophys Res, 109, 10.1029/2003jd003919, 2004.

Falkovich, A. H., Graber, E. R., Schkolnik, G., Rudich, Y., Maenhaut, W., and Artaxo, P.: Low molecular weight organic acids in aerosol particles from Rondônia, Brazil, during the biomass-burning, transition and wet periods, Atmos Chem Phys, 5, 781-797, 10.5194/acp-5-781-2005, 2005.

Fine, P. M., Chakrabarti, B., Krudysz, M., Schauer, J. J., and Sioutas, C.: Diurnal variations of individual organic compound constituents of ultrafine and accumulation mode particulate matter in the Los Angeles Basin, Environ Sci Technol, 38, 1296-1304, 10.1021/es0348389, 2004.

Fitzgerald, J. W.: Marine aerosols: A review, Atmos Environ A-Gen, 25, 533-545, 10.1016/0960-1686(91)90050-h, 1991.

Fossum, K. N., Ovadnevaite, J., Ceburnis, D., Dall'Osto, M., Marullo, S., Bellacicco, M., Simo, R., Liu, D., Flynn, M., Zuend, A., and O'Dowd, C.: Summertime Primary and Secondary Contributions to Southern Ocean Cloud Condensation Nuclei, Sci Rep, 8, 13844, 10.1038/s41598-018-32047-4, 2018.

Freedman, M. A., Hasenkopf, C. A., Beaver, M. R., and Tolbert, M. A.: Optical properties of internally mixed aerosol particles composed of dicarboxylic acids and ammonium sulfate, J Phys Chem A, 113, 13584-13592, 10.1021/jp906240y, 2009.

Fu, P. Q., Kawamura, K., Chen, J., Li, J., Sun, Y. L., Liu, Y., Tachibana, E., Aggarwal, S. G., Okuzawa, K., Tanimoto, H., Kanaya, Y., and Wang, Z. F.: Diurnal variations of organic molecular tracers and stable carbon isotopic composition in atmospheric aerosols over Mt. Tai in the North China Plain: an influence of biomass burning, Atmos Chem Phys, 12, 8359-8375, 10.5194/acp-12-8359-2012, 2012.

Gao, S., Hegg, D. A., Hobbs, P. V., Kirchstetter, T. W., Magi, B. I., and Sadilek, M.: Water-soluble organic components in aerosols associated with savanna fires in southern Africa: Identification, evolution, and distribution, J Geophys Res-Atmos, 108, 10.1029/2002jd002324, 2003.

Gao, Y., Arimoto, R., Duce, R. A., Chen, L. Q., Zhou, M. Y., and Gu, D. Y.: Atmospheric non-sea-salt sulfate, nitrate and methanesulfonate over the China Sea, J Geophys Res-Atmos, 101, 12601-12611, 10.1029/96jd00866, 1996.

Ge, C., Wang, J., Reid, J. S., Posselt, D. J., Xian, P., and Hyer, E.: Mesoscale modeling of smoke transport from equatorial Southeast Asian Maritime Continent to the Philippines: First comparison of ensemble analysis with in situ observations, J Geophys Res-Atmos, 122, 5380-5398, 10.1002/2016jd026241, 2017.

Gelencsér, and Varga: Evaluation of the atmospheric significance of multiphase reactions in atmospheric secondary organic aerosol formation, Atmos Chem Phys, 5, 2823-2831, 10.5194/acp-5-2823-2005, 2005.

Golly, B., Waked, A., Weber, S., Samake, A., Jacob, V., Conil, S., Rangognio, J., Chrétien, E., Vagnot, M. P., Robic, P. Y., Besombes, J. L., and Jaffrezo, J. L.: Organic markers and OC source apportionment for seasonal variations of PM2.5 at 5 rural sites in France, Atmos Environ, 198, 142-157, 10.1016/j.atmosenv.2018.10.027, 2019.

Gondwe, M., Krol, M., Klaassen, W., Gieskes, W., and de Baar, H.: Comparison of modeled versus measured MSA:nss SO4=ratios: A global analysis, Global Biogeochem Cy, 18, 10.1029/2003gb002144, 2004.

Graham, B., Mayol-Bracero, O. L., Guyon, P., Roberts, G. C., Decesari, S., Facchini, M. C., Artaxo, P., Maenhaut, W., Koll, P., and Andreae, M. O.: Water-soluble organic compounds in biomass burning aerosols over Amazonia1. Characterization by NMR and GC-MS, J Geophys Res, 107, LBA 14-11-LBA 14-16, 10.1029/2001jd000336, 2002.

Greenfield, S. M.: Rain scavenging of radioactive particulate matter from the atmosphere, J Meteorol, 14, 115-125, 10.1175/1520- 0469(1957)0142.0.CO, 1957.

Grosjean, D., Van Cauwenberghe, K., Schmid, J. P., Kelley, P. E., and Pitts, J. N.: Identification of C3-C10 aliphatic dicarboxylic acids in airborne particulate matter, Environ Sci Technol, 12, 313-317, 10.1021/es60139a005, 1978.

Gullett, B. K., Linak, W. P., Touati, A., Wasson, S. J., Gatica, S., and King, C. J.: Characterization of air emissions and residual ash from open burning of electronic wastes during simulated rudimentary recycling operations, J Mater Cycles Waste, 9, 69-79, 10.1007/s10163-006-0161-x, 2007.

Hanson, D. R.: Mass accommodation of H2SO4 and CH3SO3H on water-sulfuric acid solutions from 6% to 97% RH, J Phys Chem A, 109, 6919-6927, 10.1021/jp0510443, 2005.

Harrison, R. M., Beddows, D. C., and Dall'Osto, M.: PMF analysis of wide-range particle size spectra collected on a major highway, Environ Sci Technol, 45, 5522-5528, 10.1021/es2006622, 2011.

Hatakeyama, S., Ohno, M., Weng, J., Takagi, H., and Akimoto, H.: Mechanism for the formation of gaseous and particulate products from ozone-cycloalkene reactions in air, Environ Sci Technol, 21, 52-57, 10.1021/es00155a005, 1987.

Hegde, P., Kawamura, K., Girach, I., and Nair, P. R.: Characterisation of water-soluble organic aerosols at a site on the southwest coast of India, Journal of Atmospheric Chemistry, 73, 181-205, 2016.

Hilario, M. R. A., Cruz, M. T., Bañaga, P. A., Betito, G., Braun, R. A., Stahl, C., Cambaliza, M. O., Lorenzo, G. R., MacDonald, A. B., AzadiAghdam, M., Pabroa, P. C., Yee, J. R., Simpas, J. B., and Sorooshian, A.: Characterizing weekly cycles of particulate matter in a coastal megacity: The importance of a seasonal, size-resolved, and chemically-speciated analysis, J Geophys Res-Atmos, 125, 10.1029/2020JD032614, 2020a.

Hilario, M. R. A., Cruz, M. T., Cambaliza, M. O. L., Reid, J. S., Xian, P., Simpas, J. B., Lagrosas, N. D., Uy, S. N. Y., Cliff, S., and Zhao, Y.: Investigating size-segregated sources of elemental composition of particulate matter in the South China Sea during the 2011 Vasco cruise, Atmos Chem Phys, 20, 1255-1276, 10.5194/acp-20-1255-2020, 2020b.

Ho, K. F., Lee, S. C., Cao, J. J., Kawamura, K., Watanabe, T., Cheng, Y., and Chow, J. C.: Dicarboxylic acids, ketocarboxylic acids and dicarbonyls in the urban roadside area of Hong Kong, Atmos Environ, 40, 3030-3040, 10.1016/j.atmosenv.2005.11.069, 2006.

Hodshire, A. L., Campuzano-Jost, P., Kodros, J. K., Croft, B., Nault, B. A., Schroder, J. C., Jimenez, J. L., and Pierce, J. R.: The potential role of methanesulfonic acid (MSA) in aerosol formation and growth and the associated radiative forcings, Atmos Chem Phys, 19, 3137-3160, 10.5194/acp-19-3137-2019, 2019.

Hoffmann, E. H., Tilgner, A., Schrodner, R., Brauer, P., Wolke, R., and Herrmann, H.: An advanced modeling study on the impacts and atmospheric implications of multiphase dimethyl sulfide chemistry, Proc Natl Acad Sci U S A, 113, 11776-11781, 10.1073/pnas.1606320113, 2016.

Hoffmann, E. H., Tilgner, A., Vogelsberg, U., Wolke, R., and Herrmann, H.: Near-Explicit Multiphase Modeling of Halogen Chemistry in a Mixed Urban and Maritime Coastal Area, ACS Earth and Space Chem, 3, 2452-2471, 10.1021/acsearthspacechem.9b00184, 2019.

Hopke, P. K., Cohen, D. D., Begum, B. A., Biswas, S. K., Ni, B., Pandit, G. G., Santoso, M., Chung, Y.-S., Rahman, S. A., Hamzah, M. S., Davy, P., Markwitz, A., Waheed, S., Siddique, N., Santos, F. L., Pabroa, P. C. B., Seneviratne, M. C. S., Wimolwattanapun, W., Bunprapob, S.,

1061 Vuong, T. B., and Markowicz, A.: Urban air quality in the Asian region, Sci Total Environ, 409,
1062 4140, 10.1016/j.scitotenv.2011.06.028, 2011.
1063 Hsu, S. C., Liu, S. C., Huang, Y. T., Chou, C. C., Lung, S. C., Liu, T. H., Tu, J. Y., and Tsai, F.:
1064 Long-range southeastward transport of Asian biosmoke pollution: Signature detected by aerosol
1065 potassium in northern Taiwan, J Geophys Res-Atmos, 114, 10.1029/2009JD011725, 2009.
1066 Hsu, Y.-K., Holsen, T. M., and Hopke, P. K.: Comparison of hybrid receptor models to locate
1067 PCB sources in Chicago, Atmos Environ, 37, 545-562, 10.1016/S1352-2310(02)00886-5, 2003.
1068 Iijima, A., Sato, K., Yano, K., Tago, H., Kato, M., Kimura, H., and Furuta, N.: Particle size and
1069 composition distribution analysis of automotive brake abrasion dusts for the evaluation of
1070 antimony sources of airborne particulate matter, Atmos Environ, 41, 4908-4919,
1071 10.1016/j.atmosenv.2007.02.005, 2007.
1072 Kautzman, K. E., Surratt, J. D., Chan, M. N., Chan, A. W., Hersey, S. P., Chhabra, P. S.,
1073 Dalleska, N. F., Wennberg, P. O., Flagan, R. C., and Seinfeld, J. H.: Chemical composition of
1074 gas- and aerosol-phase products from the photooxidation of naphthalene, J Phys Chem A, 114,
1075 913-934, 10.1021/jp908530s, 2010.
1076 Kavouras, I. G., and Stephanou, E. G.: Particle size distribution of organic primary and
1077 secondary aerosol constituents in urban, background marine, and forest atmosphere, J Geophys
1078 Res, 107, 10.1029/2000jd000278, 2002.
1079 Kawamura, K., and Kaplan, I. R.: Motor exhaust emissions as a primary source for dicarboxylic
1080 acids in Los Angeles ambient air, Environ Sci Technol, 21, 105-110, 10.1021/es00155a014,
1081 1987.
1082 Kawamura, K., and Ikushima, K.: Seasonal changes in the distribution of dicarboxylic acids in
1083 the urban atmosphere, Environ Sci Technol, 27, 2227-2235, 10.1021/es00047a033, 2002.
1084 Kawamura, K., Imai, Y., and Barrie, L. A.: Photochemical production and loss of organic acids
1085 in high Arctic aerosols during long-range transport and polar sunrise ozone depletion events,
1086 Atmospheric Environment, 39, 599-614, 2005.
1087 Kawamura, K., and Yasui, O.: Diurnal changes in the distribution of dicarboxylic acids,
1088 ketocarboxylic acids and dicarbonyls in the urban Tokyo atmosphere, Atmos Environ, 39, 1945-
1089 1960, 10.1016/j.atmosenv.2004.12.014, 2005.
1090 Kawamura, K., Tachibana, E., Okuzawa, K., Aggarwal, S. G., Kanaya, Y., and Wang, Z. F.:
1091 High abundances of water-soluble dicarboxylic acids, ketocarboxylic acids and α-dicarbonyls in
1092 the mountaintop aerosols over the North China Plain during wheat burning season, Atmos Chem
1093 Phys, 13, 8285-8302, 10.5194/acp-13-8285-2013, 2013.
1094 Kawamura, K., and Bikkina, S.: A review of dicarboxylic acids and related compounds in
1095 atmospheric aerosols: Molecular distributions, sources and transformation, Atmos Res, 170, 140-
1096 160, 10.1016/j.atmosres.2015.11.018, 2016.
1097 Kecorius, S., Madueño, L., Vallar, E., Alas, H., Betito, G., Birmili, W., Cambaliza, M. O.,
1098 Catipay, G., Gonzaga-Cayetano, M., Galvez, M. C., Lorenzo, G., Müller, T., Simpas, J. B.,
1099 Tamayo, E. G., and Wiedensohler, A.: Aerosol particle mixing state, refractory particle number
1100 size distributions and emission factors in a polluted urban environment: Case study of Metro
1101 Manila, Philippines, Atmos Environ, 170, 169-183, 10.1016/j.atmosenv.2017.09.037, 2017.
1102 Kerminen, V.-M., Teinilä, K., Hillamo, R., and Mäkelä, T.: Size-segregated chemistry of
1103 particulate dicarboxylic acids in the Arctic atmosphere, Atmos Environ, 33, 2089-2100,
1104 10.1016/s1352-2310(98)00350-1, 1999.

1105 Kerminen, V.-M., Aurela, M., Hillamo, R. E., and Virkkula, A.: Formation of particulate MSA:
1106 deductions from size distribution measurements in the Finnish Arctic, Tellus B, 49, 159-171,
1107 10.3402/tellusb.v49i2.15959, 2017.
1108 Kim Oanh, N. T., Upadhyay, N., Zhuang, Y. H., Hao, Z. P., Murthy, D. V. S., Lestari, P.,
1109 Villarin, J. T., Chengchua, K., Co, H. X., and Dung, N. T.: Particulate air pollution in six Asian
1110 cities: Spatial and temporal distributions, and associated sources, Atmos Environ, 40, 3367-3380,
1111 10.1016/j.atmosenv.2006.01.050, 2006.
1112 Kleindienst, T. E., Jaoui, M., Lewandowski, M., Offenberg, J. H., and Docherty, K. S.: The
1113 formation of SOA and chemical tracer compounds from the photooxidation of naphthalene and
1114 its methyl analogs in the presence and absence of nitrogen oxides, Atmos Chem Phys, 12, 8711-
1115 8726, 10.5194/acp-12-8711-2012, 2012.
1116 Kobayashi, H., Matsunaga, T., Hoyano, A., Aoki, M., Komori, D., and Boonyawat, S.: Satellite
1117 estimation of photosynthetically active radiation in Southeast Asia: Impacts of smoke and cloud
1118 cover, J Geophys Res-Atmos, 109, 10.1029/2003jd003807, 2004.
1119 Kumar, S., Aggarwal, S. G., Gupta, P. K., and Kawamura, K.: Investigation of the tracers for
1120 plastic-enriched waste burning aerosols, Atmos Environ, 108, 49-58,
1121 10.1016/j.atmosenv.2015.02.066, 2015.
1122 Kundu, S., Kawamura, K., Andreae, T. W., Hoffer, A., and Andreae, M. O.: Molecular
1123 distributions of dicarboxylic acids, ketocarboxylic acids and α-dicarbonyls in biomass
1124 burning aerosols: implications for photochemical production and degradation in smoke layers,
1125 Atmos Chem Phys, 10, 2209-2225, 10.5194/acp-10-2209-2010, 2010.
1126 Kunwar, B., Kawamura, K., Fujiwara, S., Fu, P., Miyazaki, Y., and Pokhrel, A.: Dicarboxylic
1127 acids, oxocarboxylic acids and α-dicarbonyls in atmospheric aerosols from Mt. Fuji, Japan:
1128 Implication for primary emission versus secondary formation, Atmos Res, 221, 58-71,
1129 10.1016/j.atmosres.2019.01.021, 2019.
1130 Li, J., Wang, G., Zhang, Q., Li, J., Wu, C., Jiang, W., Zhu, T., and Zeng, L.: Molecular
1131 characteristics and diurnal variations of organic aerosols at a rural site in the North China Plain
1132 with implications for the influence of regional biomass burning, Atmos Chem Phys, 19, 10481-
1133 10496, 10.5194/acp-19-10481-2019, 2019.
1134 Limbeck, A., Puxbaum, H., Otter, L., and Scholes, M. C.: Semivolatile behavior of dicarboxylic
1135 acids and other polar organic species at a rural background site (Nylsvley, RSA), Atmos
1136 Environ, 35, 1853-1862, 10.1016/s1352-2310(00)00497-0, 2001.
1137 Linak, W. P., Miller, C. A., and Wendt, J. O.: Comparison of particle size distributions and
1138 elemental partitioning from the combustion of pulverized coal and residual fuel oil, J Air Waste
1139 Manag Assoc, 50, 1532-1544, 10.1080/10473289.2000.10464171, 2000.
1140 Liu, Y., Minofar, B., Desyaterik, Y., Dames, E., Zhu, Z., Cain, J. P., Hopkins, R. J., Gilles, M.
1141 K., Wang, H., Jungwirth, P., and Laskin, A.: Internal structure, hygroscopic and reactive
1142 properties of mixed sodium methanesulfonate-sodium chloride particles, Phys Chem Chem Phys,
1143 13, 11846-11857, 10.1039/c1cp20444k, 2011.
1144 Ma, L., Dadashazar, H., Braun, R. A., MacDonald, A. B., Aghdam, M. A., Maudlin, L. C., and
1145 Sorooshian, A.: Size-resolved characteristics of water-soluble particulate elements in a coastal
1146 area: Source identification, influence of wildfires, and diurnal variability, Atmos Environ, 206,
1147 72-84, 10.1016/j.atmosenv.2019.02.045, 2019.
1148 Madueño, L., Kecorius, S., Birmili, W., Müller, T., Simpas, J., Vallar, E., Galvez, M. C.,
1149 Cayetano, M., and Wiedensohler, A.: Aerosol Particle and Black Carbon Emission Factors of
1150 Vehicular Fleet in Manila, Philippines, Atmosphere, 10, 603, 10.3390/atmos10100603, 2019.

Mahowald, N., Jickells, T. D., Baker, A. R., Artaxo, P., Benitez-Nelson, C. R., Bergametti, G., Bond, T. C., Chen, Y., Cohen, D. D., Herut, B., Kubilay, N., Losno, R., Luo, C., Maenhaut, W., McGee, K. A., Okin, G. S., Siefert, R. L., and Tsukuda, S.: Global distribution of atmospheric phosphorus sources, concentrations and deposition rates, and anthropogenic impacts, Global Biogeochem Cy, 22, 10.1029/2008gb003240, 2008.

Malm, W. C., Sisler, J. F., Huffman, D., Eldred, R. A., and Cahill, T. A.: Spatial and seasonal trends in particle concentration and optical extinction in the United States, J Geophys Res-Atmos, 99, 1347-1370, 10.1029/93jd02916, 1994.

Mardi, A. H., Dadashazar, H., MacDonald, A. B., Braun, R. A., Crosbie, E., Xian, P., Thorsen, T. J., Coggon, M. M., Fenn, M. A., Ferrare, R. A., Hair, J. W., Woods, R. K., Jonsson, H. H., Flagan, R. C., Seinfeld, J. H., and Sorooshian, A.: Biomass Burning Plumes in the Vicinity of the California Coast: Airborne Characterization of Physicochemical Properties, Heating Rates, and Spatiotemporal Features, J Geophys Res-Atmos, 123, 13,560-513,582, 10.1029/2018jd029134, 2018.

Marple, V., Olson, B., Romay, F., Hudak, G., Geerts, S. M., and Lundgren, D.: Second Generation Micro-Orifice Uniform Deposit Impactor, 120 MOUDI-II: Design, Evaluation, and Application to Long-Term Ambient Sampling, Aerosol Sci. Tech., 48, 427-433, 10.1080/02786826.2014.884274, 2014.

Marsh, A., Miles, R. E. H., Rovelli, G., Cowling, A. G., Nandy, L., Dutcher, C. S., and Reid, J. P.: Influence of organic compound functionality on aerosol hygroscopicity: dicarboxylic acids, alkyl-substituents, sugars and amino acids, Atmos Chem Phys, 17, 5583-5599, 10.5194/acp-17-5583-2017, 2017.

Marsh, A., Rovelli, G., Miles, R. E. H., and Reid, J. P.: Complexity of Measuring and Representing the Hygroscopicity of Mixed Component Aerosol, J Phys Chem A, 123, 1648-1660, 10.1021/acs.jpca.8b11623, 2019.

Matsumoto, J., Olaguera, L. M. P., Nguyen-Le, D., Kubota, H., and Villafuerte, M. Q.: Climatological seasonal changes of wind and rainfall in the Philippines, Int J Climatol, 10.1002/joc.6492, 2020.

Maudlin, L. C., Wang, Z., Jonsson, H. H., and Sorooshian, A.: Impact of wildfires on size-resolved aerosol composition at a coastal California site, Atmos Environ, 119, 59-68, 10.1016/j.atmosenv.2015.08.039, 2015.

McGinty, S. M., Kapala, M. K., and Niedziela, R. F.: Mid-infrared complex refractive indices for oleic acid and optical properties of model oleic acid/water aerosols, Phys Chem Chem Phys, 11, 7998-8004, 10.1039/b905371a, 2009.

Miljevic, B., Hedayat, F., Stevanovic, S., Fairfull-Smith, K. E., Bottle, S., and Ristovski, Z.: To sonicate or not to sonicate PM filters: Reactive oxygen species generation upon ultrasonic irradiation, Aerosol Sci. Tech., 48, 1276-1284, 10.1080/02786826.2014.981330, 2014.

Mochida, M., Umemoto, N., Kawamura, K., and Uematsu, M.: Bimodal size distribution of C2-C4dicarboxylic acids in the marine aerosols, Geophys Res Lett, 30, 10.1029/2003gl017451, 2003.

Mooibroek, D., Schaap, M., Weijers, E. P., and Hoogerbrugge, R.: Source apportionment and spatial variability of PM2.5 using measurements at five sites in the Netherlands, Atmos Environ, 45, 4180-4191, 10.1016/j.atmosenv.2011.05.017, 2011.

Mora, M., Braun, R. A., Shingler, T., and Sorooshian, A.: Analysis of remotely sensed and surface data of aerosols and meteorology for the Mexico Megalopolis Area between 2003 and 2015, J Geophys Res Atmos, 122, 8705-8723, 10.1002/2017JD026739, 2017.

1197 Myhre, C. E. L., and Nielsen, C. J.: Optical properties in the UV and visible spectral region of
1198 organic acids relevant to tropospheric aerosols, Atmos Chem Phys, 4, 1759-1769, 10.5194/acp-4-
1199 1759-2004, 2004.
1200 Narukawa, M., Kawamura, K., Takeuchi, N., and Nakajima, T.: Distribution of dicarboxylic
1201 acids and carbon isotopic compositions in aerosols from 1997 Indonesian forest fires, Geophys
1202 Res Lett, 26, 3101-3104, 10.1029/1999gl010810, 1999.
1203 Neusüss, C., Pelzing, M., Plewka, A., and Herrmann, H.: A new analytical approach for size-
1204 resolved speciation of organic compounds in atmospheric aerosol particles: Methods and first
1205 results, J Geophys Res-Atmos, 105, 4513-4527, 10.1029/1999jd901038, 2000.
1206 Nguyen, D. L., Kawamura, K., Ono, K., Ram, S. S., Engling, G., Lee, C.-T., Lin, N.-H., Chang,
1207 S.-C., Chuang, M.-T., and Hsiao, T.-C.: Comprehensive PM2.5 organic molecular composition
1208 and stable carbon isotope ratios at Sonla, Vietnam: Fingerprint of biomass burning components,
1209 Aerosol Air Qual Res, 16, 2618-2634, 10.4209/aaqr.2015.07.0459 2016.
1210 Norton, R. B., Roberts, J. M., and Huebert, B. J.: Tropospheric oxalate, Geophys Res Lett, 10,
1211 517-520, 10.1029/GL010i007p00517, 1983.
1212 Ovadnevaite, J., Ceburnis, D., Leinert, S., Dall'Osto, M., Canagaratna, M., O'Doherty, S.,
1213 Berresheim, H., and O'Dowd, C.: Submicron NE Atlantic marine aerosol chemical composition
1214 and abundance: Seasonal trends and air mass categorization, J Geophys Res-Atmos, 119, 11,850-
1215 811,863, 10.1002/2013jd021330, 2014.
1216 Paatero, P., and Tapper, U.: Positive matrix factorization: A non-negative factor model with
1217 optimal utilization of error estimates of data values, Environmetrics, 5, 111-126, 1994.
1218 Pabroa, P. C. B., Santos, F. L., Morco, R. P., Racho, J. M. D., Bautista Vii, A. T., and Bucal, C.
1219 G. D.: Receptor modeling studies for the characterization of air particulate lead pollution sources
1220 in Valenzuela sampling site (Philippines), Atmos Pollut Res, 2, 213-218, 10.5094/apr.2011.027,
1221 2011.
1222 PAGASA: Termination of the southwest monsoon: http://bagong.pagasa.dost.gov.ph/press-
1223 release/30, 2018a.
1224 PAGASA: Onset of the rainy season: http://bagong.pagasa.dost.gov.ph/press-release/29#, 2018b.
1225 PAGASA: Onset of the northeast monsoon: http://bagong.pagasa.dost.gov.ph/press-release/32,
1226 2018c.
1227 PAGASA: Onset of the rainy season: http://bagong.pagasa.dost.gov.ph/press-release/50, 2019a.
1228 PAGASA: Transition to northeast monsoon: http://bagong.pagasa.dost.gov.ph/press-release/56,
1229 2019b.
1230 Paris, R., and Desboeufs, K.: Effect of atmospheric organic complexation on iron-bearing dust
1231 solubility, Atmos Chem Phys, 13, 4895-4905, 10.5194/acp-13-4895-2013, 2013.
1232 Peng, C., and Chan, C. K.: The water cycles of water-soluble organic salts of atmospheric
1233 importance, Atmos Environ, 35, 1183-1192, 10.1016/s1352-2310(00)00426-x, 2001.
1234 Peng, C., Jing, B., Guo, Y. C., Zhang, Y. H., and Ge, M. F.: Hygroscopic Behavior of
1235 Multicomponent Aerosols Involving NaCl and Dicarboxylic Acids, J Phys Chem A, 120, 1029-
1236 1038, 10.1021/acs.jpca.5b09373, 2016.
1237 Pereira, W. E., Rostad, C. E., Taylor, H. E., and Klein, J. M.: Characterization of organic
1238 contaminants in environmental samples associated with Mount St. Helens 1980 volcanic
1239 eruption, Environ Sci Technol, 16, 387-396, 10.1021/es00101a005, 1982.
1240 Prabhakar, G., Sorooshian, A., Toffol, E., Arellano, A. F., and Betterton, E. A.: Spatiotemporal
1241 Distribution of Airborne Particulate Metals and Metalloids in a Populated Arid Region, Atmos
1242 Environ, 92, 339-347, 10.1016/j.atmosenv.2014.04.044, 2014.

Pratt, K. A., Murphy, S. M., Subramanian, R., DeMott, P. J., Kok, G. L., Campos, T., Rogers, D. C., Prenni, A. J., Heymsfield, A. J., Seinfeld, J. H., and Prather, K. A.: Flight-based chemical characterization of biomass burning aerosols within two prescribed burn smoke plumes, Atmos Chem Phys, 11, 12549-12565, 10.5194/acp-11-12549-2011, 2011.

Prenni, A. J., DeMott, P. J., Kreidenweis, S. M., Sherman, D. E., Russell, L. M., and Ming, Y.: The Effects of Low Molecular Weight Dicarboxylic Acids on Cloud Formation, J Phys Chem A, 105, 11240-11248, 10.1021/jp012427d, 2001.

PSA: Highlights of the Philippine population 2015 census of population: https://psa.gov.ph/content/highlights-philippine-population-2015-census-population, access: January 7, 2016.

Ramachandran, S., and Rajesh, T. A.: Black carbon aerosol mass concentrations over Ahmedabad, an urban location in western India: Comparison with urban sites in Asia, Europe, Canada, and the United States, J Geophys Res, 112, 10.1029/2006jd007488, 2007.

Ran, L., Deng, Z. Z., Wang, P. C., and Xia, X. A.: Black carbon and wavelength-dependent aerosol absorption in the North China Plain based on two-year aethalometer measurements, Atmos Environ, 142, 132-144, 10.1016/j.atmosenv.2016.07.014, 2016.

Reff, A., Eberly, S. I., and Bhave, P. V.: Receptor modeling of ambient particulate matter data using positive matrix factorization: review of existing methods, J Air Waste Manag Assoc, 57, 146-154, 10.1080/10473289.2007.10465319, 2007.

Reid, J. S., Hobbs, P. V., Ferek, R. J., Blake, D. R., Martins, J. V., Dunlap, M. R., and Liousse, C.: Physical, chemical, and optical properties of regional hazes dominated by smoke in Brazil, J Geophys Res-Atmos, 103, 32059-32080, 10.1029/98jd00458, 1998.

Reid, J. S., Koppmann, R., Eck, T. F., and Eleuterio, D. P.: A review of biomass burning emissions part II: intensive physical properties of biomass burning particles, Atmos Chem Phys, 5, 799-825, 10.5194/acp-5-799-2005, 2005.

Reid, J. S., Hyer, E. J., Johnson, R. S., Holben, B. N., Yokelson, R. J., Zhang, J., Campbell, J. R., Christopher, S. A., Di Girolamo, L., Giglio, L., Holz, R. E., Kearney, C., Miettinen, J., Reid, E. A., Turk, F. J., Wang, J., Xian, P., Zhao, G., Balasubramanian, R., Chew, B. N., Janjai, S., Lagrosas, N., Lestari, P., Lin, N.-H., Mahmud, M., Nguyen, A. X., Norris, B., Oanh, N. T. K., Oo, M., Salinas, S. V., Welton, E. J., and Liew, S. C.: Observing and understanding the Southeast Asian aerosol system by remote sensing: An initial review and analysis for the Seven Southeast Asian Studies (7SEAS) program, Atmos Res, 122, 403-468, 10.1016/j.atmosres.2012.06.005, 2013.

Reid, J. S., Xian, P., Holben, B. N., Hyer, E. J., Reid, E. A., Salinas, S. V., Zhang, J., Campbell, J. R., Chew, B. N., Holz, R. E., Kuciauskas, A. P., Lagrosas, N., Posselt, D. J., Sampson, C. R., Walker, A. L., Welton, E. J., and Zhang, C.: Aerosol meteorology of the Maritime Continent for the 2012 7SEAS southwest monsoon intensive study – Part 1: regional-scale phenomena, Atmos Chem Phys, 16, 14041-14056, 10.5194/acp-16-14041-2016, 2016.

Rogge, W. F., Mazurek, M. A., Hildemann, L. M., Cass, G. R., and Simoneit, B. R. T.: Quantification of urban organic aerosols at a molecular level: Identification, abundance and seasonal variation, Atmos Environ A-Gen, 27, 1309-1330, 10.1016/0960-1686(93)90257-y, 1993.

Rolph, G., Stein, A., and Stunder, B.: Real-time Environmental Applications and Display sYstem: READY, Environ Modell Softw, 95, 210-228, 10.1016/j.envsoft.2017.06.025, 2017.

Rose, C., Chaumerliac, N., Deguillaume, L., Perroux, H., Mouchel-Vallon, C., Leriche, M., Patryl, L., and Armand, P.: Modeling the partitioning of organic chemical species in cloud phases with CLEPS (1.1), Atmos Chem Phys, 18, 2225-2242, 10.5194/acp-18-2225-2018, 2018.

Russell, L. M., Maria, S. F., and Myneni, S. C. B.: Mapping organic coatings on atmospheric particles, Geophys Res Lett, 29, 26-21-26-24, 10.1029/2002gl014874, 2002.

Saltzman, E. S., Savoie, D. L., Zika, R. G., and Prospero, J. M.: Methane sulfonic acid in the marine atmosphere, J Geophys Res-Oceans, 88, 10897-10902, 10.1029/JC088iC15p10897, 1983.

Sareen, N., Carlton, A. G., Surratt, J. D., Gold, A., Lee, B., Lopez-Hilfiker, F. D., Mohr, C., Thornton, J. A., Zhang, Z., Lim, Y. B., and Turpin, B. J.: Identifying precursors and aqueous organic aerosol formation pathways during the SOAS campaign, Atmos Chem Phys, 16, 14409-14420, 10.5194/acp-16-14409-2016, 2016.

Saxena, P., and Hildemann, L. M.: Water-soluble organics in atmospheric particles: A critical review of the literature and application of thermodynamics to identify candidate compounds, J Atmos Chem, 24, 57-109, 10.1007/bf00053823, 1996.

Schlosser, J. S., Braun, R. A., Bradley, T., Dadashazar, H., MacDonald, A. B., Aldhaif, A. A., Aghdam, M. A., Mardi, A. H., Xian, P., and Sorooshian, A.: Analysis of aerosol composition data for western United States wildfires between 2005 and 2015: Dust emissions, chloride depletion, and most enhanced aerosol constituents, J Geophys Res-Atmos, 122, 8951-8966, 2017.

Seinfeld, J. H., and Pandis, S. N.: Atmospheric chemistry and physics, 3rd ed., Wiley-Interscience, New York, 2016.

Sempére, R., and Kawamura, K.: Comparative distributions of dicarboxylic acids and related polar compounds in snow, rain and aerosols from urban atmosphere, Atmos Environ, 28, 449-459, 10.1016/1352-2310(94)90123-6, 1994.

Siffert, C., and Sulzberger, B.: Light-induced dissolution of hematite in the presence of oxalate. A case study, Langmuir, 7, 1627-1634, 10.1021/la00056a014, 1991.

Simoneit, B. R., Medeiros, P. M., and Didyk, B. M.: Combustion products of plastics as indicators for refuse burning in the atmosphere, Environ Sci Technol, 39, 6961-6970, 10.1021/es050767x, 2005.

Simpas, J., Lorenzo, G., and Cruz, M.: Monitoring Particulate Matter Levels and Composition for Source Apportionment Study in Metro Manila, Philippines, in: Improving Air Quality in Asian Developing Countries: Compilation of Research Findings, edited by: Kim Oanh, N. T., 239-261, 2014.

Singh, M., Jaques, P. A., and Sioutas, C.: Size distribution and diurnal characteristics of particle-bound metals in source and receptor sites of the Los Angeles Basin, Atmos Environ, 36, 1675-1689, 10.1016/s1352-2310(02)00166-8, 2002.

Song, J., Zhao, Y., Zhang, Y., Fu, P., Zheng, L., Yuan, Q., Wang, S., Huang, X., Xu, W., Cao, Z., Gromov, S., and Lai, S.: Influence of biomass burning on atmospheric aerosols over the western South China Sea: Insights from ions, carbonaceous fractions and stable carbon isotope ratios, Environ Pollut, 242, 1800-1809, 10.1016/j.envpol.2018.07.088, 2018.

Sorooshian, A., Varutbangkul, V., Brechtel, F. J., Ervens, B., Feingold, G., Bahreini, R., Murphy, S. M., Holloway, J. S., Atlas, E. L., Buzorius, G., Jonsson, H., Flagan, R. C., and Seinfeld, J. H.: Oxalic acid in clear and cloudy atmospheres: Analysis of data from International Consortium for Atmospheric Research on Transport and Transformation 2004, J Geophys Res-Atmos, 111, 10.1029/2005jd006880, 2006.

1332   Sorooshian, A., Lu, M. L., Brechtel, F. J., Jonsson, H., Feingold, G., Flagan, R. C., and Seinfeld,
1333   J. H.: On the source of organic acid aerosol layers above clouds, Environ Sci Technol, 41, 4647-
1334   4654, 10.1021/es0630442, 2007a.
1335   Sorooshian, A., Ng, N. L., Chan, A. W. H., Feingold, G., Flagan, R. C., and Seinfeld, J. H.:
1336   Particulate organic acids and overall water-soluble aerosol composition measurements from the
1337   2006 Gulf of Mexico Atmospheric Composition and Climate Study (GoMACCS), J Geophys
1338   Res-Atmos, 112, 10.1029/2007jd008537, 2007b.
1339   Sorooshian, A., Hersey, S., Brechtel, F. J., Corless, A., Flagan, R. C., and Seinfeld, J. H.: Rapid,
1340   Size-Resolved Aerosol Hygroscopic Growth Measurements: Differential Aerosol Sizing and
1341   Hygroscopicity Spectrometer Probe (DASH-SP), Aerosol Sci. Tech., 42, 445-464,
1342   10.1080/02786820802178506, 2008.
1343   Sorooshian, A., Padró, L. T., Nenes, A., Feingold, G., McComiskey, A., Hersey, S. P., Gates, H.,
1344   Jonsson, H. H., Miller, S. D., Stephens, G. L., Flagan, R. C., and Seinfeld, J. H.: On the link
1345   between ocean biota emissions, aerosol, and maritime clouds: Airborne, ground, and satellite
1346   measurements off the coast of California, Global Biogeochem Cy, 23, 10.1029/2009gb003464,
1347   2009.
1348   Sorooshian, A., Murphy, S. M., Hersey, S., Bahreini, R., Jonsson, H., Flagan, R. C., and
1349   Seinfeld, J. H.: Constraining the contribution of organic acids and AMSm/z44 to the organic
1350   aerosol budget: On the importance of meteorology, aerosol hygroscopicity, and region, Geophys
1351   Res Lett, 37, 10.1029/2010gl044951, 2010.
1352   Sorooshian, A., Wonaschutz, A., Jarjour, E. G., Hashimoto, B. I., Schichtel, B. A., and Betterton,
1353   E. A.: An aerosol climatology for a rapidly growing arid region (southern Arizona): Major
1354   aerosol species and remotely sensed aerosol properties, J Geophys Res Atmos, 116, 16,
1355   10.1029/2011JD016197, 2011.
1356   Sorooshian, A., Wang, Z., Coggon, M. M., Jonsson, H. H., and Ervens, B.: Observations of sharp
1357   oxalate reductions in stratocumulus clouds at variable altitudes: organic acid and metal
1358   measurements during the 2011 E-PEACE campaign, Environ Sci Technol, 47, 7747-7756,
1359   10.1021/es4012383, 2013.
1360   Sorooshian, A., Crosbie, E., Maudlin, L. C., Youn, J. S., Wang, Z., Shingler, T., Ortega, A. M.,
1361   Hersey, S., and Woods, R. K.: Surface and airborne measurements of organosulfur and
1362   methanesulfonate over the Western United States and coastal areas, J Geophys Res Atmos, 120,
1363   8535-8548, 10.1002/2015JD023822, 2015.
1364   Stahl, C., Cruz, M. T., Banaga, P. A., Betito, G., Braun, R. A., Aghdam, M. A., Cambaliza, M.
1365   O., Lorenzo, G. R., MacDonald, A. B., Pabroa, P. C., Yee, J. R., Simpas, J. B., and Sorooshian,
1366   A.: An annual time series of weekly size-resolved aerosol properties in the megacity of Metro
1367   Manila, Philippines, Sci Data, 7, 128, 10.1038/s41597-020-0466-y, 2020a.
1368   Stahl, C., Cruz, M. T., Banaga, P. A., Betito, G., Braun, R. A., Aghdam, M. A., Cambaliza, M.
1369   O., Lorenzo, G. R., MacDonald, A. B., Pabroa, P. C., Yee, J. R., Simpas, J. B., and Sorooshian,
1370   A., An annual time series of weekly size-resolved aerosol properties in the megacity of Metro
1371   Manila, Philippines, figshare, https://doi.org/10.6084/m9.figshare.11861859, 2020b
1372   Stein, A. F., Draxler, R. R., Rolph, G. D., Stunder, B. J. B., Cohen, M. D., and Ngan, F.:
1373   NOAA's HYSPLIT Atmospheric Transport and Dispersion Modeling System, B Am Meteorol
1374   Soc, 96, 2059-2077, 10.1175/bams-d-14-00110.1, 2015.
1375   Streets, D. G., Carmichael, G. R., and Arndt, R. L.: Sulfur dioxide emissions and sulfur
1376   deposition from international shipping in Asian waters, Atmos Environ, 31, 1573-1582,
1377   10.1016/s1352-2310(96)00204-x, 1997.

Streets, D. G., Guttikunda, S. K., and Carmichael, G. R.: The growing contribution of sulfur emissions from ships in Asian waters, 1988–1995, Atmos Environ, 34, 4425-4439, 10.1016/s1352-2310(00)00175-8, 2000.

Sullivan, R. C., and Prather, K. A.: Investigations of the diurnal cycle and mixing state of oxalic acid in individual particles in Asian aerosol outflow, Environ Sci Technol, 41, 8062-8069, 10.1021/es071134g, 2007.

Takahashi, K., Nansai, K., Tohno, S., Nishizawa, M., Kurokawa, J.-i., and Ohara, T.: Production-based emissions, consumption-based emissions and consumption-based health impacts of PM2.5 carbonaceous aerosols in Asia, Atmos Environ, 97, 406-415, 10.1016/j.atmosenv.2014.04.028, 2014.

Tang, M., Guo, L., Bai, Y., Huang, R.-J., Wu, Z., Wang, Z., Zhang, G., Ding, X., Hu, M., and Wang, X.: Impacts of methanesulfonate on the cloud condensation nucleation activity of sea salt aerosol, Atmos Environ, 201, 13-17, 10.1016/j.atmosenv.2018.12.034, 2019.

Tang, M. J., Whitehead, J., Davidson, N. M., Pope, F. D., Alfarra, M. R., McFiggans, G., and Kalberer, M.: Cloud condensation nucleation activities of calcium carbonate and its atmospheric ageing products, Phys Chem Chem Phys, 17, 32194-32203, 10.1039/c5cp03795f, 2015.

Thepnuan, D., Chantara, S., Lee, C. T., Lin, N. H., and Tsai, Y. I.: Molecular markers for biomass burning associated with the characterization of PM2.5 and component sources during dry season haze episodes in Upper South East Asia, Sci Total Environ, 658, 708-722, 10.1016/j.scitotenv.2018.12.201, 2019.

Tsai, Y. I., Kuo, S.-C., Young, L.-H., Hsieh, L.-Y., and Chen, P.-T.: Atmospheric dry plus wet deposition and wet-only deposition of dicarboxylic acids and inorganic compounds in a coastal suburban environment, Atmos Environ, 89, 696-706, 10.1016/j.atmosenv.2014.03.013, 2014.

van Drooge, B. L., and Grimalt, J. O.: Particle size-resolved source apportionment of primary and secondary organic tracer compounds at urban and rural locations in Spain, Atmos Chem Phys, 15, 7735-7752, 10.5194/acp-15-7735-2015, 2015.

van Pinxteren, M., Fiedler, B., van Pinxteren, D., Iinuma, Y., Körtzinger, A., and Herrmann, H.: Chemical characterization of sub-micrometer aerosol particles in the tropical Atlantic Ocean: marine and biomass burning influences, J Atmos Chem, 72, 105-125, 10.1007/s10874-015-9307-3, 2015.

Vasconcellos, P. C., Souza, D. Z., Sanchez-Ccoyllo, O., Bustillos, J. O., Lee, H., Santos, F. C., Nascimento, K. H., Araujo, M. P., Saarnio, K., Teinila, K., and Hillamo, R.: Determination of anthropogenic and biogenic compounds on atmospheric aerosol collected in urban, biomass burning and forest areas in Sao Paulo, Brazil, Sci Total Environ, 408, 5836-5844, 10.1016/j.scitotenv.2010.08.012, 2010.

Wang, G., Xie, M., Hu, S., Gao, S., Tachibana, E., and Kawamura, K.: Dicarboxylic acids, metals and isotopic compositions of C and N in atmospheric aerosols from inland China: implications for dust and coal burning emission and secondary aerosol formation, Atmos Chem Phys, 10, 6087-6096, 10.5194/acp-10-6087-2010, 2010.

Wang, G., Chen, C., Li, J., Zhou, B., Xie, M., Hu, S., Kawamura, K., and Chen, Y.: Molecular composition and size distribution of sugars, sugar-alcohols and carboxylic acids in airborne particles during a severe urban haze event caused by wheat straw burning, Atmos Environ, 45, 2473-2479, 10.1016/j.atmosenv.2011.02.045, 2011.

Wang, G., Kawamura, K., Cheng, C., Li, J., Cao, J., Zhang, R., Zhang, T., Liu, S., and Zhao, Z.: Molecular distribution and stable carbon isotopic composition of dicarboxylic acids,

ketocarboxylic acids, and alpha-dicarbonyls in size-resolved atmospheric particles from Xi'an City, China, Environ Sci Technol, 46, 4783-4791, 10.1021/es204322c, 2012.

Wang, G., Kawamura, K., Xie, M., Hu, S., Li, J., Zhou, B., Cao, J., and An, Z.: Selected water-soluble organic compounds found in size-resolved aerosols collected from urban, mountain and marine atmospheres over East Asia, Tellus B, 63, 371-381, 10.1111/j.1600-0889.2011.00536.x, 2017.

Wang, J., Ge, C., Yang, Z., Hyer, E. J., Reid, J. S., Chew, B.-N., Mahmud, M., Zhang, Y., and Zhang, M.: Mesoscale modeling of smoke transport over the Southeast Asian Maritime Continent: Interplay of sea breeze, trade wind, typhoon, and topography, Atmos Res, 122, 486-503, 10.1016/j.atmosres.2012.05.009, 2013.

Wang, Y. Q., Zhang, X. Y., and Draxler, R. R.: TrajStat: GIS-based software that uses various trajectory statistical analysis methods to identify potential sources from long-term air pollution measurement data, Environ Modell Softw, 24, 938-939, 10.1016/j.envsoft.2009.01.004, 2009.

Warneck, P.: Multi-Phase Chemistry of C2 and C3 Organic Compounds in the Marine Atmosphere, J Atmos Chem, 51, 119-159, 10.1007/s10874-005-5984-7, 2005.

Wasson, S. J., Linak, W. P., Gullett, B. K., King, C. J., Touati, A., Huggins, F. E., Chen, Y., Shah, N., and Huffman, G. P.: Emissions of chromium, copper, arsenic, and PCDDs/Fs from open burning of CCA-treated wood, Environ Sci Technol, 39, 8865-8876, 10.1021/es050891g, 2005.

Wonaschuetz, A., Sorooshian, A., Ervens, B., Chuang, P. Y., Feingold, G., Murphy, S. M., de Gouw, J., Warneke, C., and Jonsson, H. H.: Aerosol and gas re-distribution by shallow cumulus clouds: An investigation using airborne measurements, J Geophys Res-Atmos, 117, 10.1029/2012jd018089, 2012.

Wonaschütz, A., Hersey, S. P., Sorooshian, A., Craven, J. S., Metcalf, A. R., Flagan, R. C., and Seinfeld, J. H.: Impact of a large wildfire on water-soluble organic aerosol in a major urban area: the 2009 Station Fire in Los Angeles County, Atmos Chem Phys, 11, 8257-8270, 10.5194/acp-11-8257-2011, 2011.

Xian, P., Reid, J. S., Atwood, S. A., Johnson, R. S., Hyer, E. J., Westphal, D. L., and Sessions, W.: Smoke aerosol transport patterns over the Maritime Continent, Atmos Res, 122, 469-485, 10.1016/j.atmosres.2012.05.006, 2013.

Xu, J., Tian, Y., Cheng, C., Wang, C., Lin, Q., Li, M., Wang, X., and Shi, G.: Characteristics and source apportionment of ambient single particles in Tianjin, China: The close association between oxalic acid and biomass burning, Atmos Res, 237, 104843, 10.1016/j.atmosres.2020.104843, 2020.

Xue, H., Khalizov, A. F., Wang, L., Zheng, J., and Zhang, R.: Effects of dicarboxylic acid coating on the optical properties of soot, Phys Chem Chem Phys, 11, 7869-7875, 10.1039/b904129j, 2009.

Yamasoe, M. A., Artaxo, P., Miguel, A. H., and Allen, A. G.: Chemical composition of aerosol particles from direct emissions of vegetation fires in the Amazon Basin: water-soluble species and trace elements, Atmos Environ, 34, 1641-1653, 10.1016/s1352-2310(99)00329-5, 2000.

Yang, H., Yu, J. Z., Ho, S. S. H., Xu, J., Wu, W.-S., Wan, C. H., Wang, X., Wang, X., and Wang, L.: The chemical composition of inorganic and carbonaceous materials in PM2.5 in Nanjing, China, Atmos Environ, 39, 3735-3749, 10.1016/j.atmosenv.2005.03.010, 2005.

Yao, X., Fang, M., and Chan, C. K.: Size distributions and formation of dicarboxylic acids in atmospheric particles, Atmos Environ, 36, 2099-2107, 10.1016/s1352-2310(02)00230-3, 2002.

1468   Yao, X., Lau, A. P. S., Fang, M., Chan, C. K., and Hu, M.: Size distributions and formation of
1469   ionic species in atmospheric particulate pollutants in Beijing, China: 2—dicarboxylic acids,
1470   Atmos Environ, 37, 3001-3007, 10.1016/s1352-2310(03)00256-5, 2003.
1471   Yu, J. Z., Huang, X.-F., Xu, J., and Hu, M.: When Aerosol Sulfate Goes Up, So Does
1472   Oxalate: Implication for the Formation Mechanisms of Oxalate, Environ Sci Technol, 39, 128-
1473   133, 10.1021/es049559f, 2005.
1474   Yuan, H., Wang, Y., and Zhuang, G.: MSA in Beijing aerosol, Chinese Sci Bull, 49, 1020-1025,
1475   10.1007/bf03184031, 2004.
1476   Zeng, G., Kelley, J., Kish, J. D., and Liu, Y.: Temperature-dependent deliquescent and
1477   efflorescent properties of methanesulfonate sodium studied by ATR-FTIR spectroscopy, J Phys
1478   Chem A, 118, 583-591, 10.1021/jp405896y, 2014.
1479   Ziemba, L. D., Griffin, R. J., Whitlow, S., and Talbot, R. W.: Characterization of water-soluble
1480   organic aerosol in coastal New England: Implications of variations in size distribution, Atmos
1481   Environ, 45, 7319-7329, 10.1016/j.atmosenv.2011.08.022, 2011.
1482   Zuo, Y.: Kinetics of photochemical/chemical cycling of iron coupled with organic substances in
1483   cloud and fog droplets, Geochim Cosmochim Acta, 59, 3123-3130, 10.1016/0016-
1484   7037(95)00201-A, 1995.

1485

Table 1: Seasonal concentrations (ng m^{-3}) of organic acids and MSA for all (0.056 – 18 μm), submicrometer (0.056 – 1 μm), and supermicrometer (1 – 18 μm) sizes measured in Metro Manila from July 2018 to October 2019. n = number of sets.

Size/Species		All (n = 54)		SWM18 (n = 11)		Transitional (n = 3)		NEM (n = 27)		SWM19 (n = 13)	
		Range	Mean (SD)	Range	Mean (SD)	Range	Mean (SD)	Range	Mean (SD)	Range	Mean (SD)
All: 0.056 - 18 μm	Phthalate	0 - 67.02	9 (14)	1.97 - 67.02	17 (25)	17.36 - 45.30	27 (16)	0 - 14.72	4.8 (4.4)	0-25.03	5.7 (7.4)
	Adipate	0 - 43.83	7.6 (9.4)	0 - 20.18	9.1 (8.8)	0.24 - 19.56	8 (10)	0 - 13.00	4.2 (3.8)	0 - 43.83	13 (15)
	Succinate	0 - 116.28	10 (22)	0 - 116.28	22 (43)	0 - 14.31	7.6 (7.2)	0 - 62.83	7 (14)	0 - 20.14	4.7 (7.4)
	Maleate	0 - 119.19	10 (20)	2.56 - 58.39	19 (15)	0.19 - 8.45	3.8 (4.2)	0 - 14.42	1.7 (3.7)	2.30 - 119.19	19 (34)
	Oxalate	37.67 - 472.82	149 (94)	49.83 - 472.82	178 (139)	179.42 - 365.10	252 (99)	51.62 - 421.82	144 (76)	37.67 - 214.62	110 (62)
	MSA	0.10 - 23.33	5.4 (5.2)	2.77 - 23.33	10.0 (6.6)	0.16 - 16.14	5.6 (9.2)	0.10 - 7.45	3.1 (2.0)	0.84 - 17.52	6.3 (5.4)
0.056 - 1 μm	Phthalate	0 - 64.53	6 (13)	0.51 - 64.53	15 (24)	9.14 - 39.62	20 (17)	0 - 9.38	1.6 (2.5)	0 - 8.51	2.7 (3.1)
	Adipate	0 - 31.57	4.3 (5.8)	0 - 15.94	6.1 (6.3)	0 - 10.99	5.5 (5.5)	0 - 10.64	2.5 (3.2)	0 - 31.57	6.1 (8.8)
	Succinate	0 - 108.47	7 (20)	0 - 108.47	19 (39)	0 - 13.54	7.3 (6.8)	0 - 52.42	4 (10)	0 - 15.68	4.3 (6.6)
	Maleate	0 - 108.65	9 (18)	2.56 - 57.73	18 (15)	0.19 - 8.45	3.8 (4.2)	0 - 14.42	1.6 (3.6)	2.30 - 108.65	18 (31)
	Oxalate	16.21 - 318.49	93 (62)	29.96 - 256.72	108 (75)	96.84 - 250.78	166 (78)	26.11 - 318.49	91 (58)	16.21 - 151.79	70 (40)
	MSA	0 - 21.32	5.0 (4.9)	2.41 - 21.32	9.3 (6.2)	0.08 - 15.58	5.3 (8.9)	0 - 7.45	2.9 (2.1)	0.84 - 16.22	5.7 (5.1)
1-18 μm	Phthalate	0 - 16.52	3.1 (3.3)	0 - 4.07	2.0 (1.7)	5.43 - 9.03	6.7 (2.0)	0 - 9.42	3.2 (2.6)	0 - 16.52	3.0 (5.0)
	Adipate	0 - 26.00	3.3 (4.9)	0 - 7.87	3.0 (3.2)	0 - 8.56	2.9 (4.9)	0 - 8.07	1.7 (2.2)	0 - 26.00	7.1 (8.0)
	Succinate	0 - 21.18	2.2 (4.5)	0 - 16.02	3.1 (4.9)	0 - 0.77	0.3 (0.4)	0 - 21.18	2.9 (5.4)	0 - 5.33	0.4 (1.5)
	Maleate	0 - 10.54	0.4 (1.5)	0 - 2.30	0.3 (0.7)	0	0	0 - 0.45	0.02 (0.09)	0 - 10.54	1.2 (2.9)
	Oxalate	6.27 - 216.10	55 (39)	19.87 - 216.10	70 (67)	62.90 - 114.32	87 (26)	18.51 - 104.88	53 (23)	6.27 - 103.58	41 (29)
	MSA	0 - 2.00	0.4 (0.5)	0 - 2.00	0.8 (0.6)	0 - 0.56	0.2 (0.3)	0 - 1.58	0.2 (0.4)	0 - 1.93	0.6 (0.6)

1489 **Table 2:** Contributions of the five positive matrix factorization (PMF) source factors to each
1490 individual organic acid and MSA.

	Combustion	Biomass Burning	Crustal	Sea Salt	Waste Processing
Phthalate	27.4 %	49.5 %	13.3 %	9.9 %	0 %
Adipate	32.9 %	26.4 %	35.9 %	4.7 %	0 %
Succinate	0 %	90.3 %	9.7 %	0 %	0 %
Maleate	69.7 %	0 %	0.2 %	0 %	30.1 %
Oxalate	32.9 %	25.4 %	31.2 %	0 %	10.5 %
MSA	57.4 %	41.2 %	0.1 %	0 %	1.4 %

1491

1492

Table 3: Pearson's correlation matrices (r values) of water-soluble species for submicrometer (0.056 – 1.0 µm) and supermicrometer (1.0 – 18 µm) sizes. Blank boxes indicate p-values exceeding 0.05 and thus deemed to be statistically insignificant. Ad – adipate, Su – succinate, Ma – maleate, Ox – oxalate, Ph – phthalate. A similar correlation matrix for the full size range (0.056 – 18 µm) is in Table S6.

< 1 µm

	Al	Ti	K	Rb	V	Ni	As	Cd	Pb	Na	Cl	NO3	SO4	MSA	Ad	Su	Ma	Ox	Ph
Al	1.00																		
Ti		1.00																	
K	0.91		1.00																
Rb	0.44		0.48	1.00															
V		0.28		0.36	1.00														
Ni		0.47		0.40	0.89	1.00													
As							1.00												
Cd					0.64	0.68		1.00											
Pb	0.41		0.32	0.27	0.28	0.40		0.42	1.00										
Na										1.00									
Cl	0.90		0.99	0.39					0.30		1.00								
NO3	0.76		0.82	0.28						0.84		1.00							
SO4				0.42	0.48	0.40							1.00						
MSA				0.39									0.60	1.00					
Ad															1.00				
Su		0.31		0.67									0.45	0.67	0.33	1.00			
Ma															0.32		1.00		
Ox		0.35		0.70	0.47	0.53							0.72	0.47		0.69		1.00	
Ph		0.37		0.53									0.39	0.67	0.45	0.82		0.57	1.00
	Al	Ti	K	Rb	V	Ni	As	Cd	Pb	Na	Cl	NO3	SO4	MSA	Ad	Su	Ma	Ox	Ph

> 1 µm

|	Al	Ti	K	Rb	V	Ni	As	Cd	Pb	Na	Cl	NO3	SO4	MSA	Ad	Su	Ma	Ox	Ph
Al	1.00																		
Ti	0.56	1.00																	
K			1.00																
Rb	0.62		0.48	1.00															
V		0.40		0.31	1.00														
Ni		0.30				1.00													
As		0.37			0.33		1.00												
Cd					0.66	0.41	0.34	1.00											
Pb	0.43	0.45		0.36	0.51	0.45		0.65	1.00										
Na	0.49	0.42								1.00									
Cl	0.45	0.48								0.90	1.00								
NO3	0.38			0.32	0.41					0.64	0.30	1.00							
SO4	0.39		0.81	0.64						0.37	0.29	0.36	1.00						
MSA										0.32				1.00					
Ad															1.00				
Su	0.39			0.28						0.30						1.00			
Ma															0.57		1.00		
Ox	0.59	0.29		0.48						0.45			0.59	0.35		0.45		1.00	
Ph		0.29									0.34				0.30				1.00
	Al	Ti	K	Rb	V	Ni	As	Cd	Pb	Na	Cl	NO3	SO4	MSA	Ad	Su	Ma	Ox	Ph
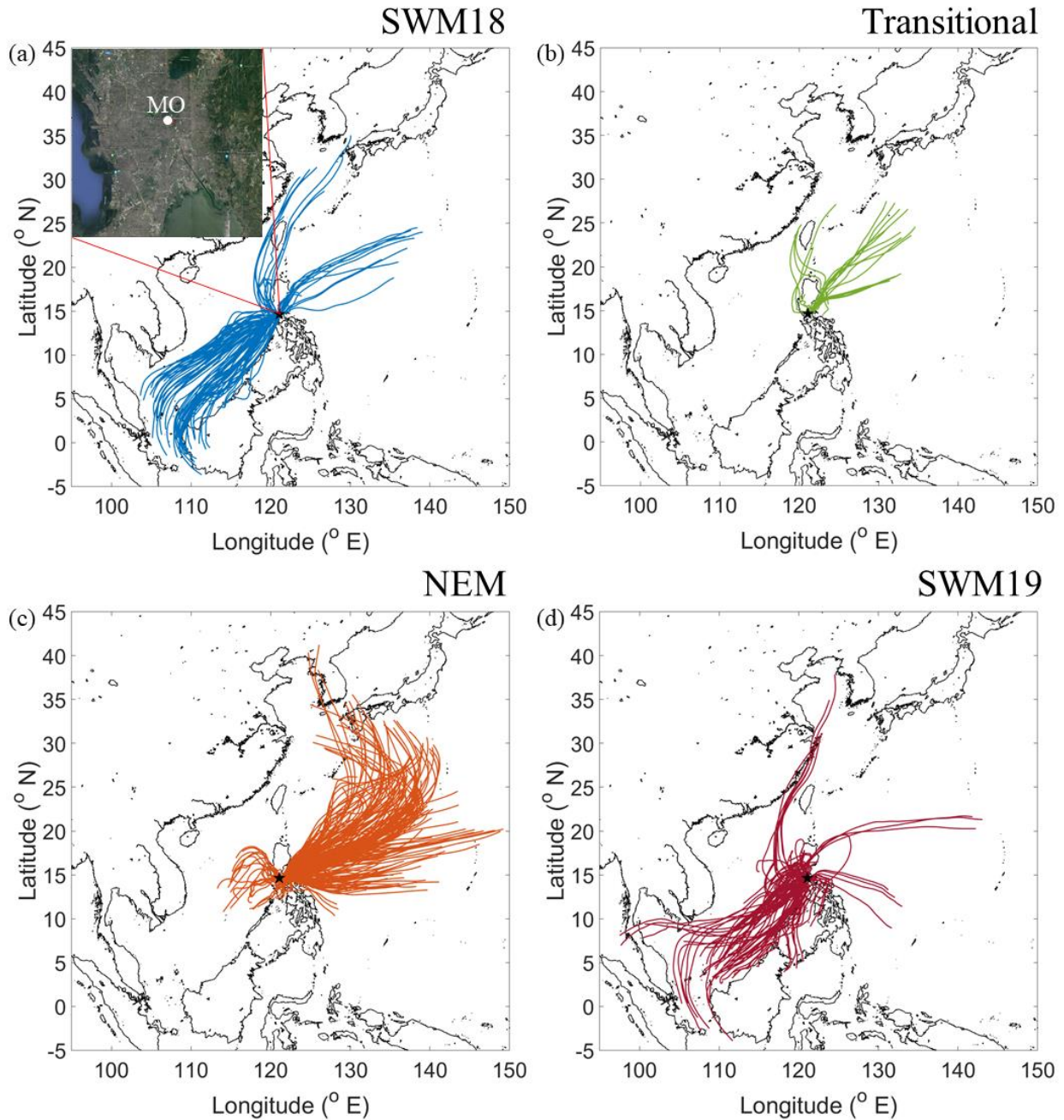
Figure 1: HYSPLIT back-trajectories for four seasons: (a) 2018 southwest monsoon (SWM18), (b) Transitional period, (c) northeast monsoon (NEM), and (d) 2019 southwest monsoon (SWM19). Results shown are based on 72-hour back-trajectories collected every 6 h during sampling periods. The top left corner of panel (a) zooms in on Metro Manila with Manila Observatory (MO) marked. The black star in each panel represents the sampling site. Map data: © Google Earth, Maxar Technologies, CNES/Airbus, Data SIO, NOAA, U.S. Navy, NGA, GEBCO.
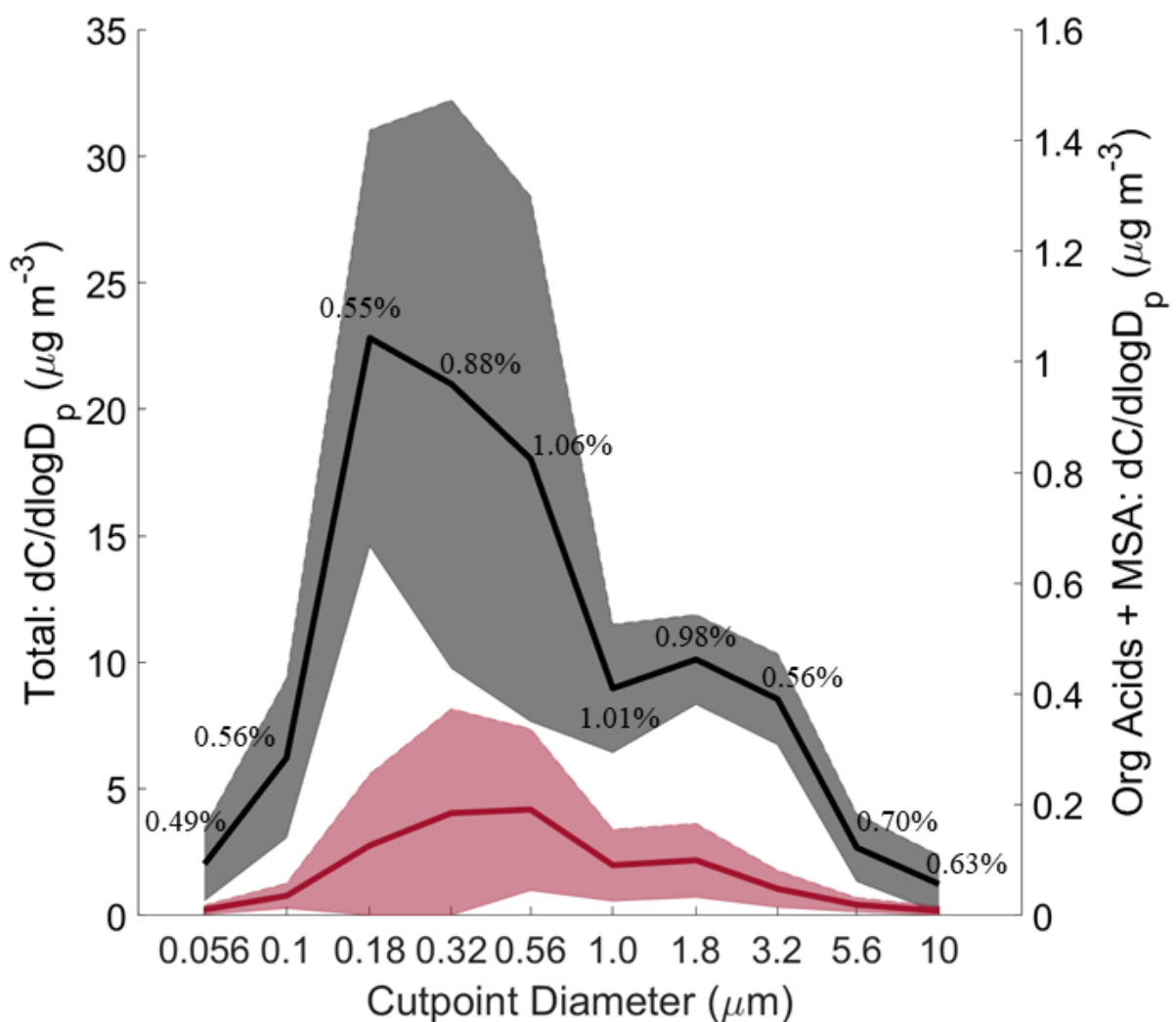
Figure 2: Size-resolved comparison of total mass versus the sum of measured organic acids and MSA. The black curve represents total mass and the red curve represents the summed organic acids and MSA. Solid lines are the averages and shaded areas are one standard deviation. These plots were made based on data from the 11 MOUDI chemical sets with accompanying gravimetric measurements. The average percent contribution of the organic acids and MSA to total mass is provided for each size bin. Refer to Fig. S1 for the seasonally-resolved version of this figure.

1517
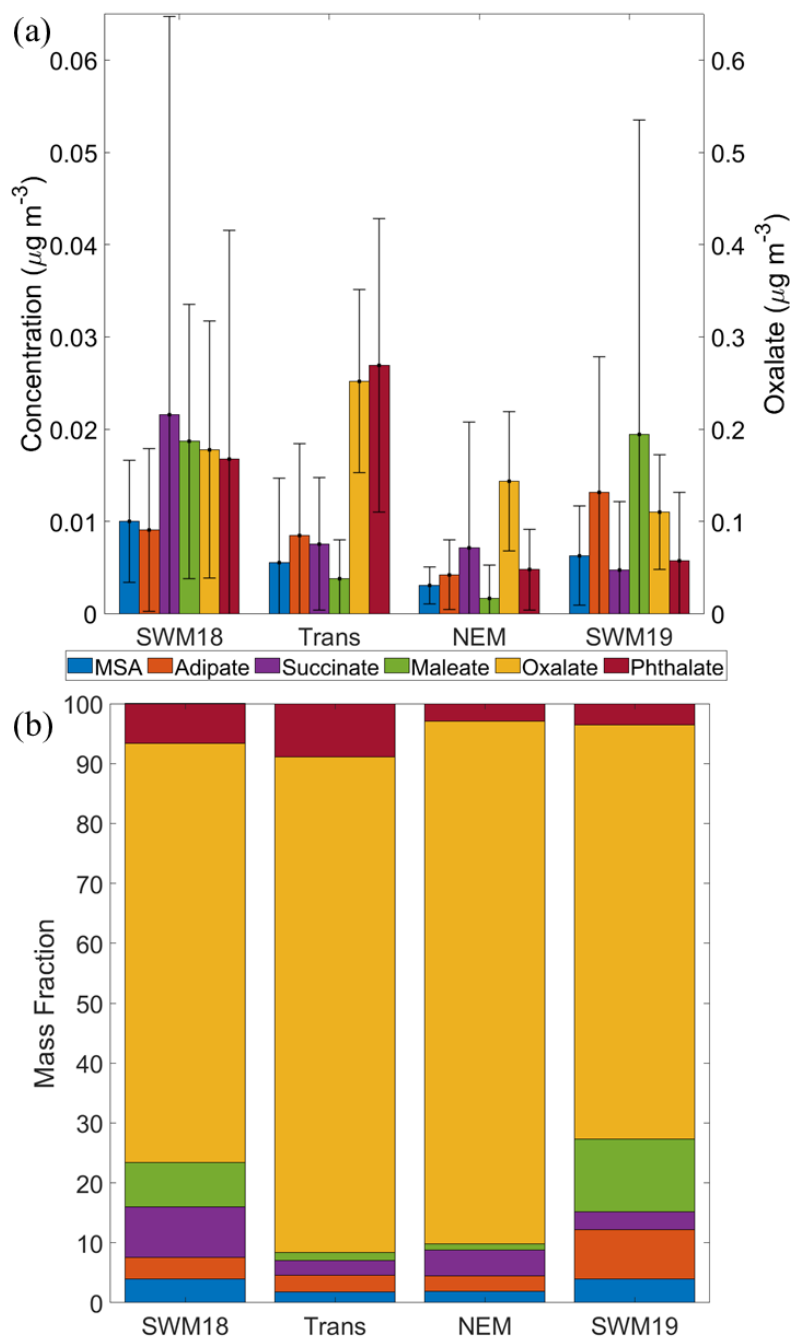
Figure 3: (a) Average concentrations (0.056 – 18 μm) for (left y-axis) MSA, adipate, succinate, maleate, and phthalate, in addition to (right y-axis) oxalate. Black bars represent one standard deviation. (b) Percentage relative mass abundance of organic acids and MSA separated based on season.

1522
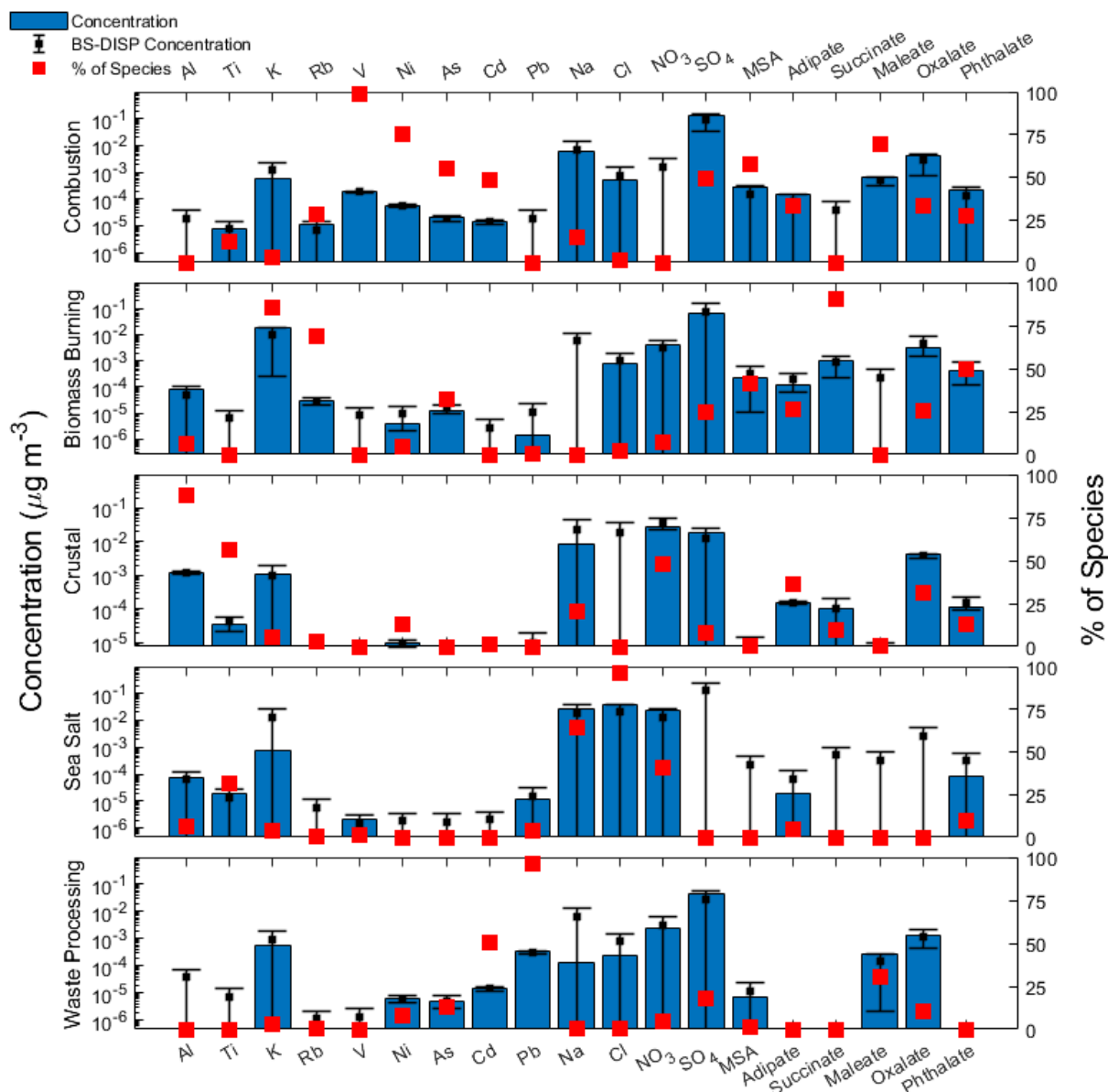
Figure 4: Source factor profiles from positive matrix factorization (PMF) analysis. Blue bars represent the mass concentration contributed to the respective factor, red filled squares represent the percentage of total species associated with that source factor, and black squares with error bars represent the average, 5th, and 95th percentiles of bootstrapping with displacement (BS-DISP) values.

1530
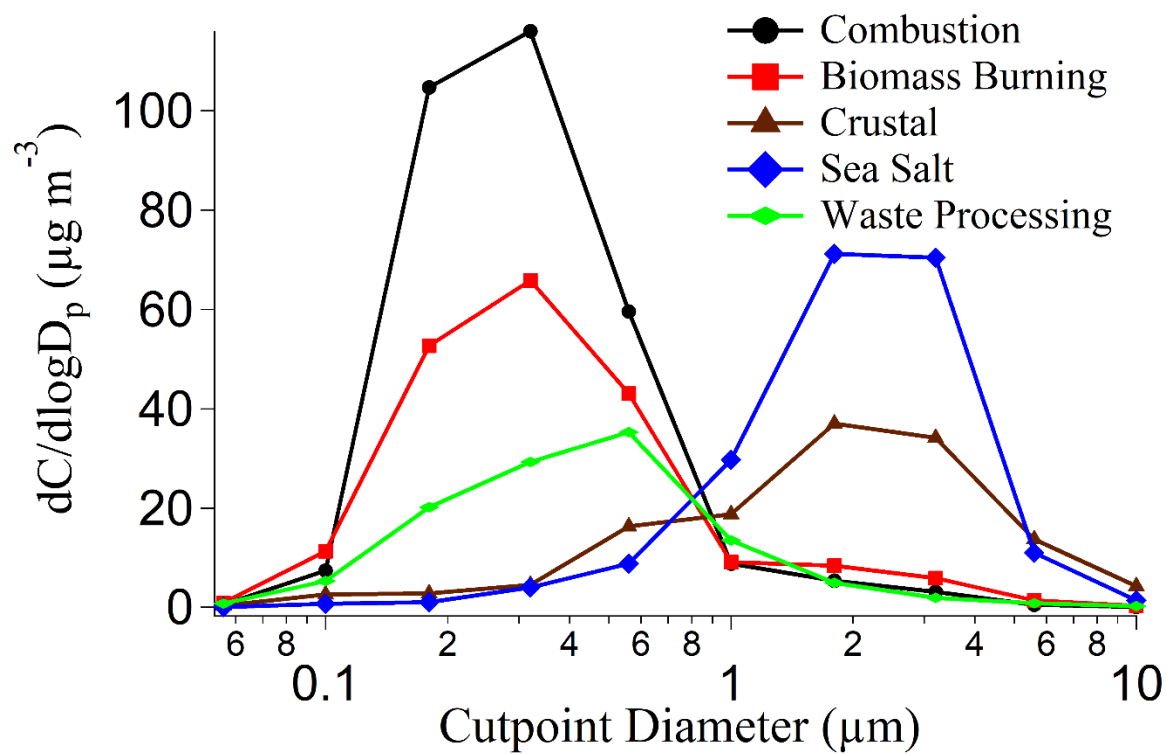
1531 **Figure 5:** Reconstructed mass size distributions of positive matrix factorization (PMF) factors.

1532

1533
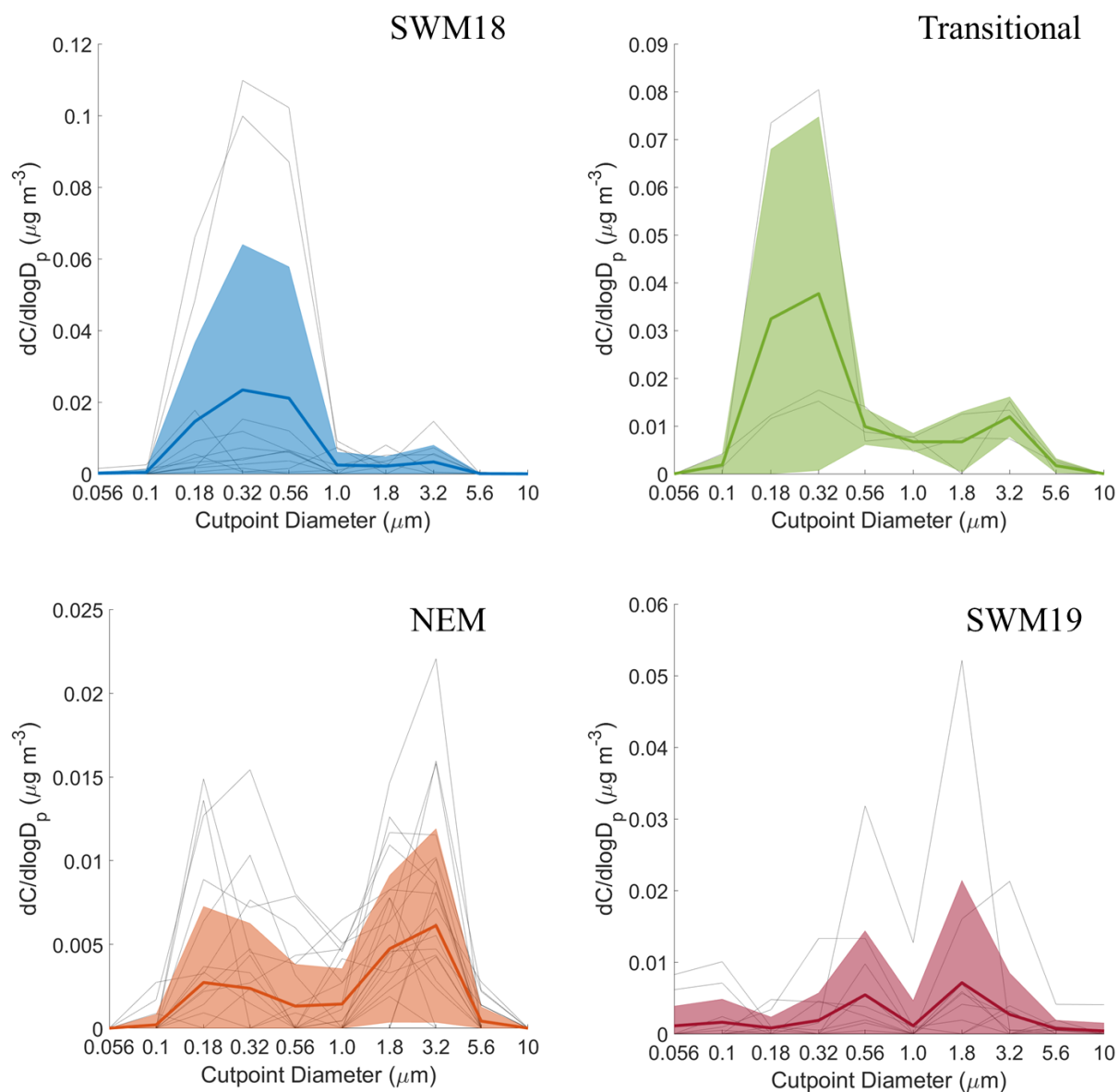
Figure 6: Seasonal size distributions of phthalate. Gray lines represent individual sets, dark colored lines are the average of all seasonal distributions, and transparent colored areas represent one standard deviation. Note that the range of concentrations presented on the y-axis for each season varies.
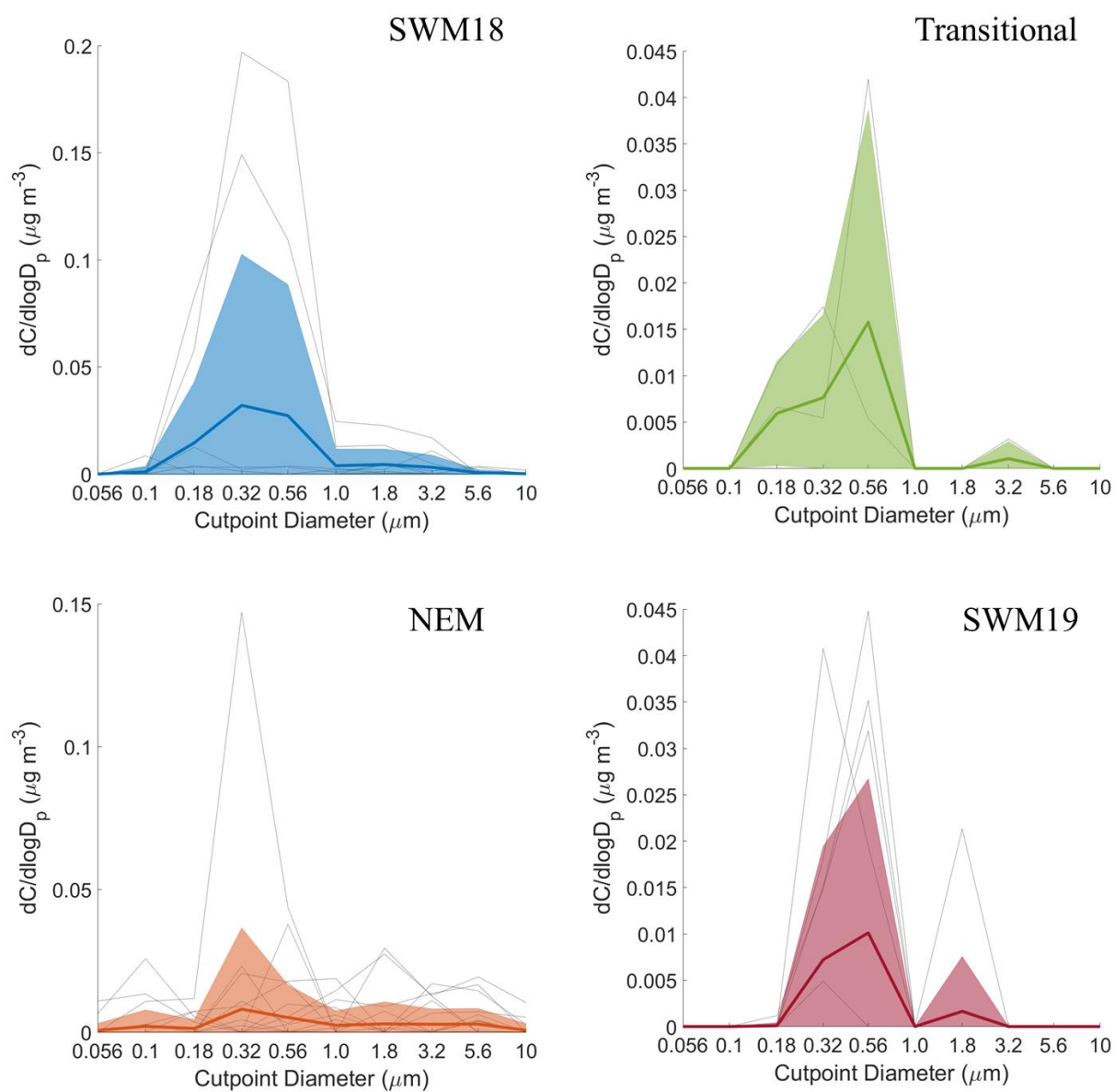
1538

1539
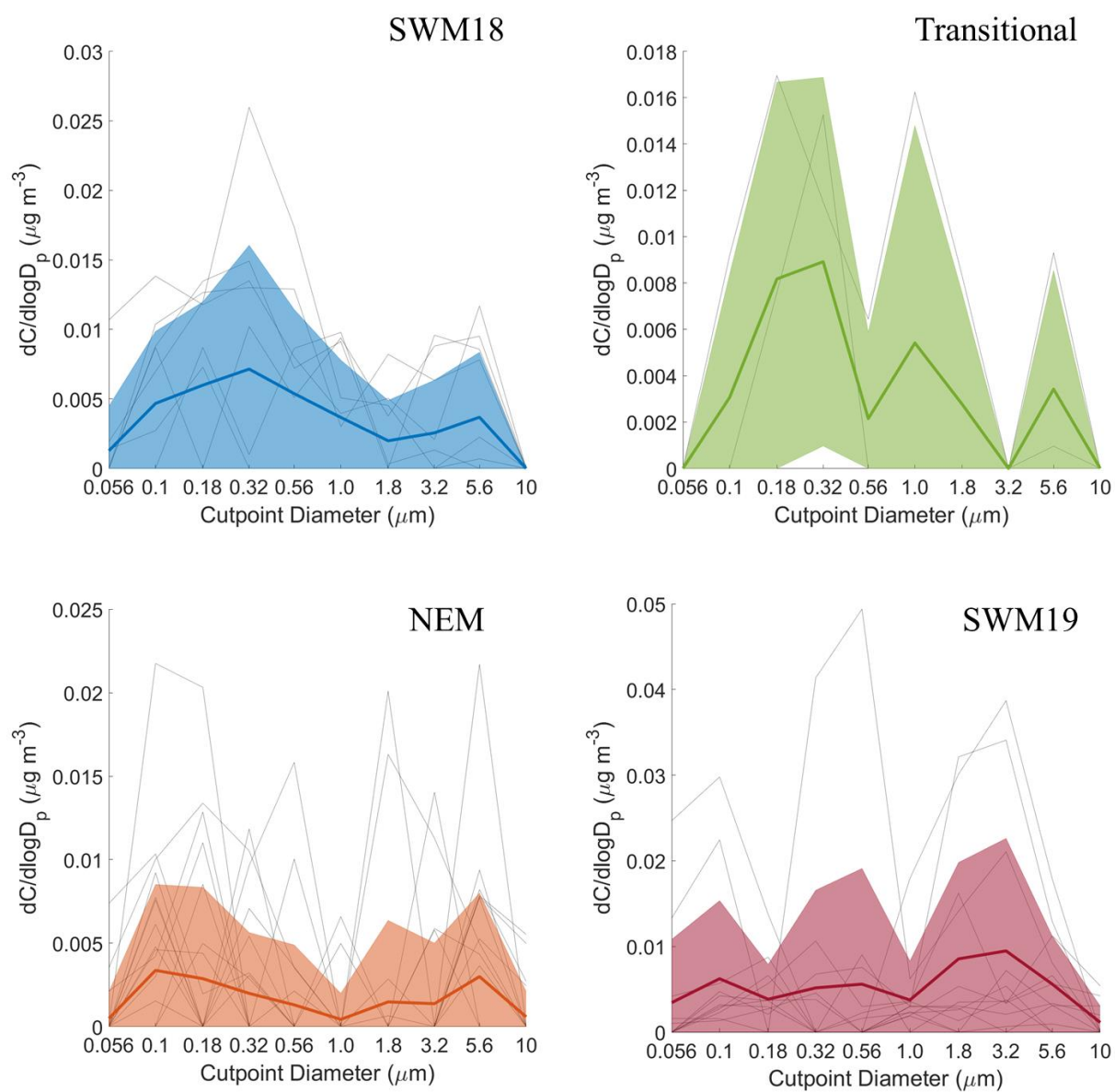
1540 **Figure 7:** Same as Fig. 6 but for adipate.

1541

1542

Figure 8: Same as Fig. 6 but for succinate.
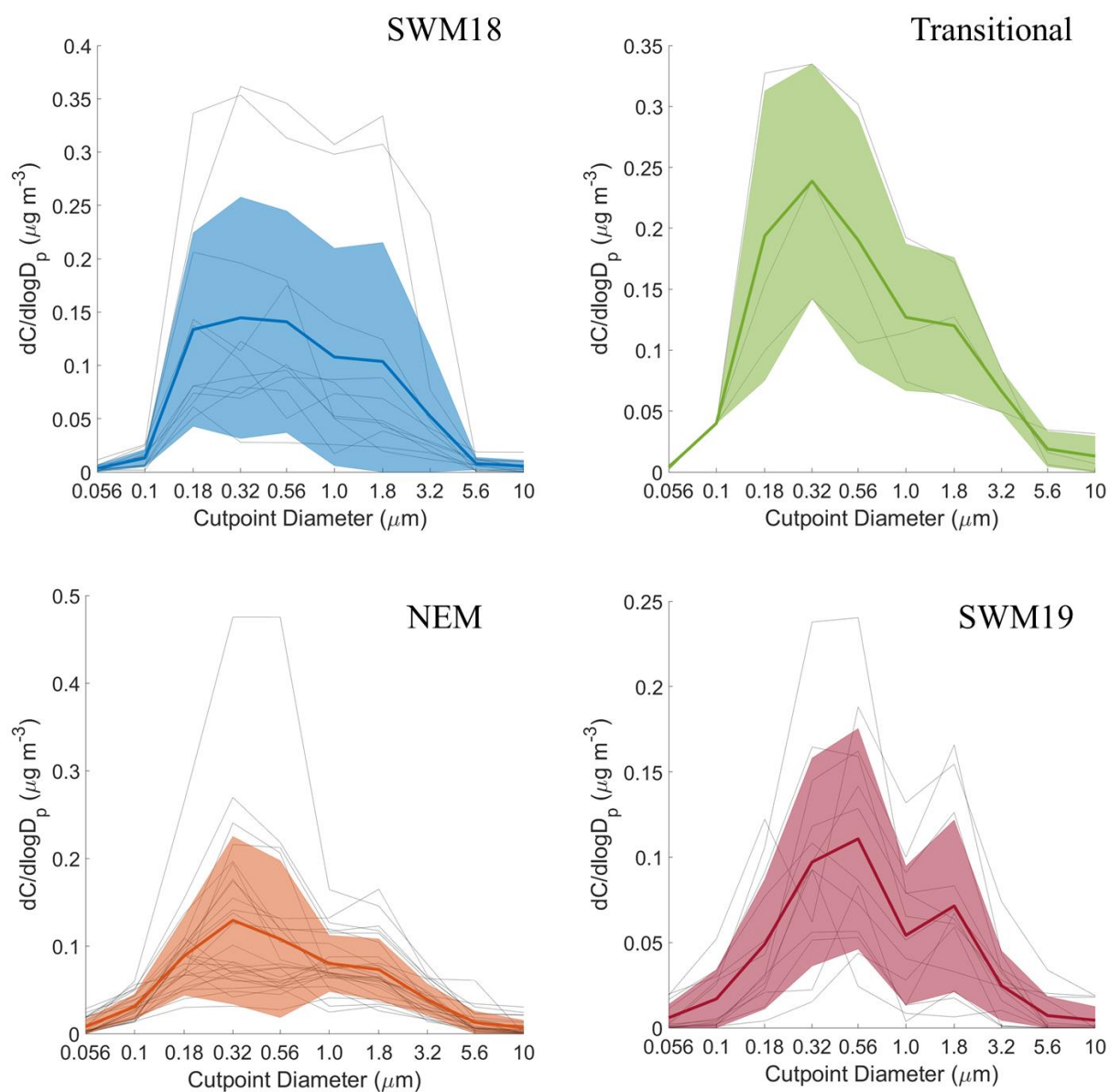
1544
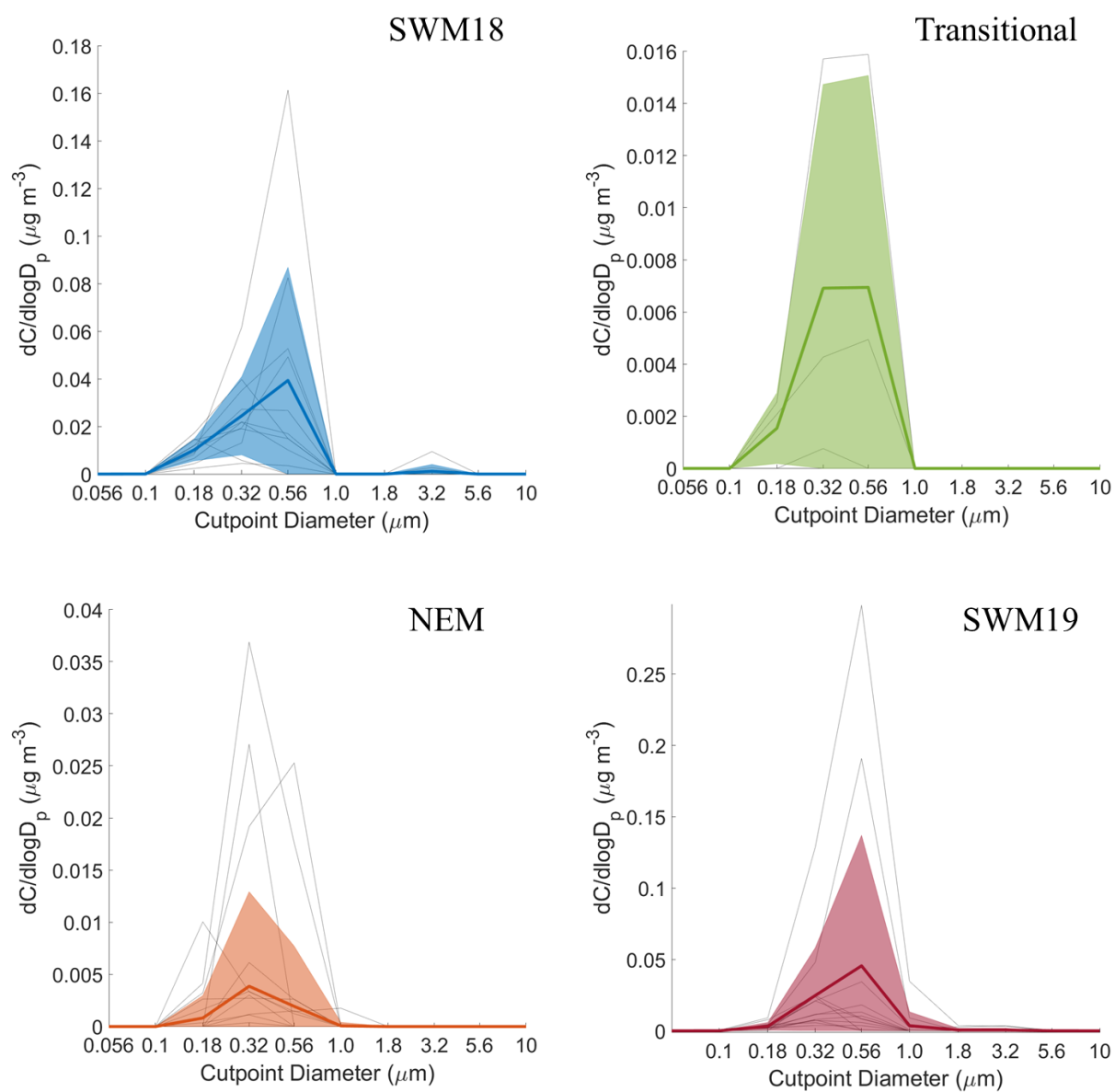
Figure 9: Same as Fig. 6 but for maleate.

1546

1547

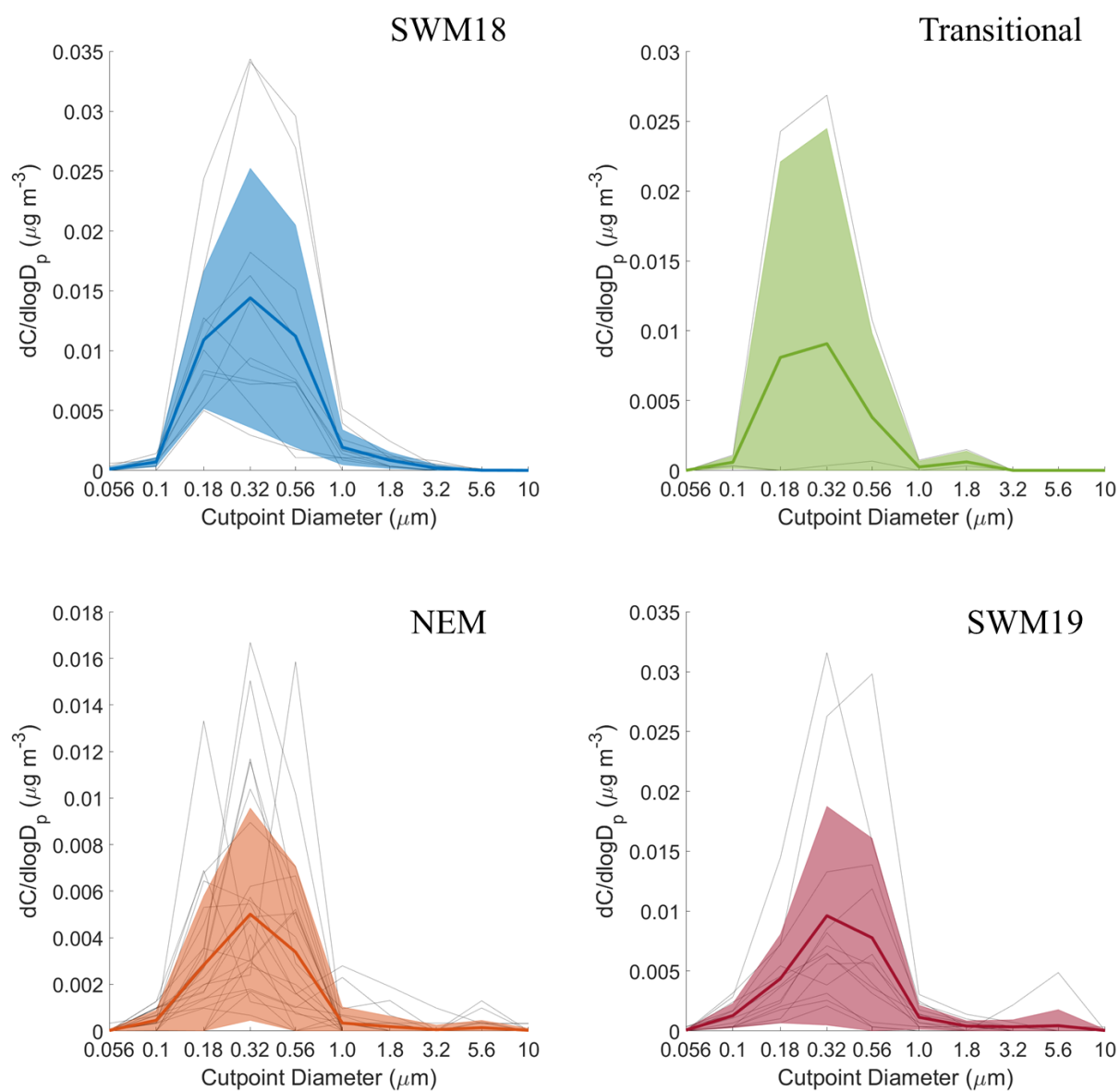**Figure 10:** Same as Fig. 6 but for oxalate.

1549
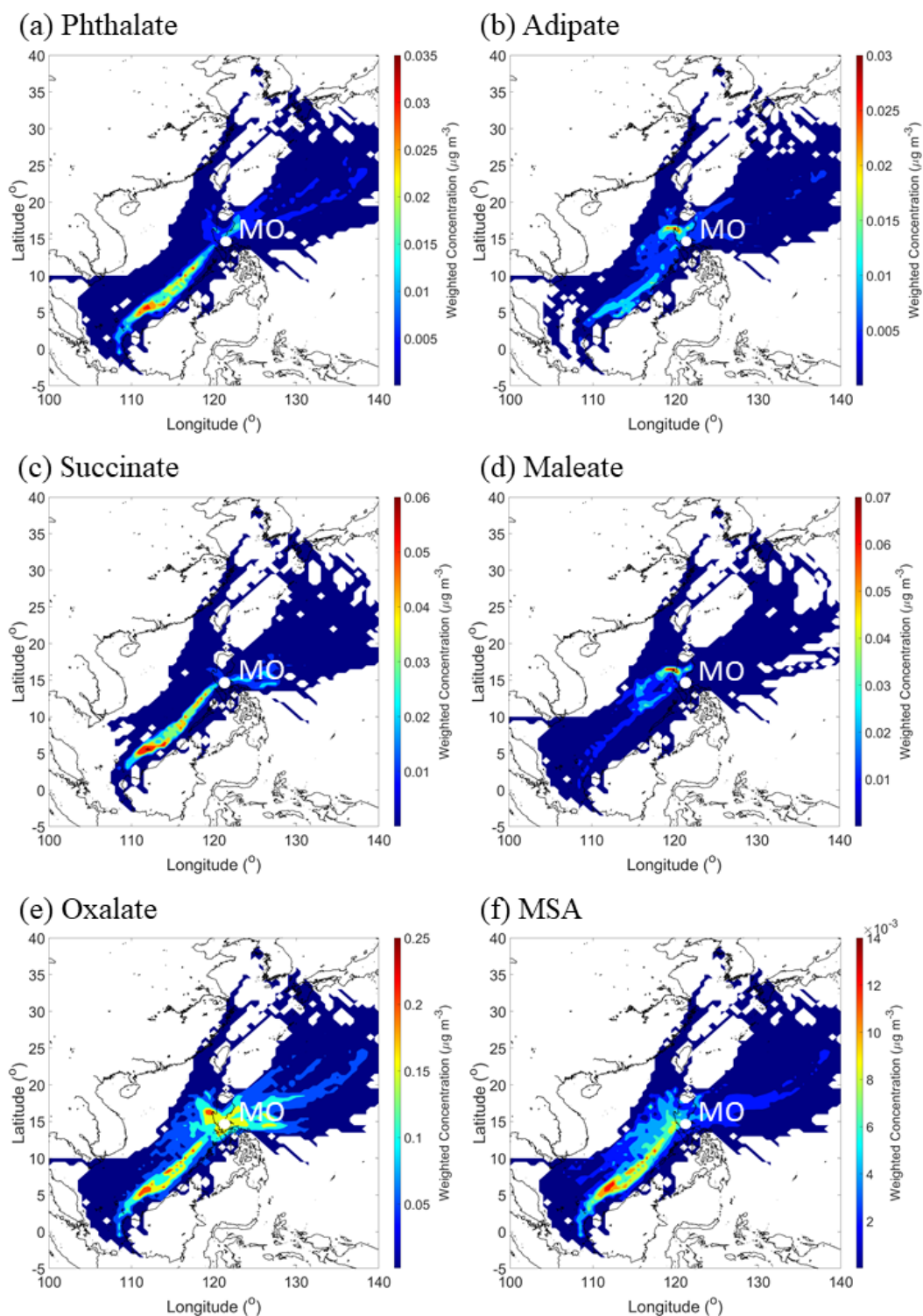
Figure 11: Same as Fig. 6 but for MSA.

1554

Figure 12: CWT maps of (a-e) individual organic acids and (f) MSA over the entire sampling
period. These results are based on all MOUDI sizes (0.056 – 18 μm). Maps showing the seasonal
results for each organic acid and MSA are shown in the Supplement (Figs. S3 – S8).